Aalto University
School of Chemical
Technology

School of Chemical Technology
Degree Programme of Materials Science and Engineering

Ville Rontu

ATOMIC LAYER DEPOSITION OF NIOBIUM NITRIDE THIN FILMS

Master's thesis for the degree of Master of Science in Technology submitted for inspection, Espoo, 07 November, 2014.

Supervisor Professor Sami Franssila

Instructor D.Sci. (Tech.) Riikka Puurunen

Aalto University
School of Chemical
Technology

Aalto University, P.O. BOX 11000, 00076 AALTO
www.aalto.fi

Abstract of master's thesis

Author Ville Rontu		
Title of thesis Atomic Layer Deposition of Niobium Nitride Thin Films		
Department Materials Science and Engineering		
Professorship Materials Science		**Code of professorship** MT-45
Thesis supervisor Prof. Sami Franssila		
Thesis advisor(s) / Thesis examiner(s) D.Sc. (Tech.) Riikka Puurunen		
Date 07.11.2014	**Number of pages** 81	**Language** English

Abstract

Niobium nitride thin films have been usually deposited by reactive magnetron sputtering. Atomic layer deposition (ALD) has emerged as viable candidate for growth of ultrathin films. Its benefits include conformal deposition and nanometer scale thickness control. So far deposition of cubic NbN phase has been realized by ALD from $NbCl_5$ and NH_3 only with help of zinc as an additional reducing agent or by PEALD from organometallic precursors. In this work we developed deposition processes for recently acquired ALD tool aiming for deposition of NbN from $NbCl_5$ without zinc.

We deposited NbN_x thin films from $NbCl_5$ using NH_3, H_2 and NH_3 as separate pulses; NH_3-plasma; H_2/N_2-plasma with varying flow rate ratios; and H_2-plasma. PEALD depositions in this work are the first published PEALD processes for NbN using $NbCl_5$ as a precursor. Thermally deposited films using NH_3 had resistivity of 650 μΩcm at best and growth rate varied from 0.34–0.52 Å/cycle. Resistivity is slightly higher than the best, 550–600 μΩcm, reported for similar process. Also GPC is higher than typically reported 0.25 Å/cycle. Films were clean having less than 1 at% impurities for films grown at 500°C. Cl-content increased from 0.3 at% to 1.8 at% as deposition temperature decreased from 500°C to 400°C. Nb/N ratios in the films were close to 0.8. Films grown with plasma typically exhibited even higher GPC, 0.5–0.85 Å/cycle. Exception to this was film grown on top of amorphous AlN which had growth rate of 0.35 Å/cycle. The best resistivity obtained for plasma processes was 490 μΩcm. ToF-ERDA measurements from H_2-plasma grown film revealed incorporation of nitrogen into the film from carrier gas lines. None of the grown films exhibited superconductivity.

It was determined that NH_3 has insufficient reducing power to create stoichiometric NbN and that use of H_2 to replace zinc as additional reducing agent would require higher temperatures. Deposition of superconductive NbN films should be possible with plasma-enhancement after changes to the ALD equipment is made in order to fully operate under argon atmosphere.

Keywords Atomic layer deposition, niobium nitride

Aalto-yliopisto
Kemian tekniikan korkeakoulu

Aalto-yliopisto, PL 11000, 00076 AALTO
www.aalto.fi

Diplomityön tiivistelmä

Tekijä Ville Rontu	
Työn nimi NbN ohutkalvojen kasvatus atomikerroskasvatusmenetelmällä	
Laitos Materiaalitekniikka	
Professuuri Materiaalitiede	**Professuurikoodi** MT-45
Työn valvoja Prof. Sami Franssila	
Työn ohjaaja(t)/Työn tarkastaja(t) TkT Riikka Puurunen	
Päivämäärä 07.11.2014 **Sivumäärä** 81	**Kieli** Englanti

Tiivistelmä

Niobiumnitridi ohutkalvoja on tavallisesti kasvatettu reaktiivisella magnetronisputteroinnilla. Atomikerroskasvatusmenetelmästä (Atomic layer deposition, ALD) on tullut varteenotettava kandidaatti erittäin ohuiden ohutkalvojen kasvatukseen. Sen etuina on muunmuassa konformaalinen kasvu ja mahdollisuus paksuuden kontrolloimiseen nanometrin mittaluokassa. Tähän asti kiderakenteeltaan kuutiollisia NbN ohutkalvoja on saatu kasvatettua ALD:llä $NbCl_5$:stä ja ammoniakista ainoastaan käyttämällä sinkkiä lisäpelkistimenä lähtöainepulssien välissä. Tämän työn tavoitteena on kehittää NbN ohutkalvojen kasvatusprosessi uudelle ALD-laitteelle käyttäen $NbCl_5$:a ilman sinkkiä.

Kasvatimme NbN_x-ohutkalvoja $NbCl_5$:sta käyttäen muina lähtöaineina ammoniakkia; vetyä ja ammoniakkia erillisinä pulsseina; ammoniakkiplasmaa; typpi-vety-plasmaa vaihtelevalla typen ja vedyn virtaus suhteilla; ja vety-plasmaa. Tässä työssä tehdyt PEALD NbN prosessit ovat ensimmäiset PEALD NbN prosessit, joissa on käytetty $NbCl_5$ lähtöaineena. Ohutkalvoilla, jotka kasvatettiin käyttäen ammoniakkia, paras havaittu resistiivisyys oli 650 μΩcm ja kasvunopeus vaihteli 0,34 ja 0,52 Å/sykli välillä. Havaittu resistiivisyys on hieman suurempi kuin kirjallisuudessa havaittu resistiivisyys vastaavalle prosessille joka on 550–600 μΩcm. Samoin kasvunopeus on suurempi kuin kirjallisuudessa havaittu 0.25 Å/sykli. Kalvot olivat erittäin puhtaita. 500 °C kasvatetuissa kalvoissa alle 1 at% epäpuhtauksia. Kloorin määrä kalvoissa havaittiin riippuvan kasvatuslämpötilasta. Klooripitoisuus 400 °C kasvatetuissa kalvoissa oli 1.8 at% ja se laski 0.3 at%:in, kun kasvatuslämpötila nostettiin 500°C:een. Niobiumin suhde typpeen kalvoissa oli noin 0.8. Plasman kanssa kasvatetuilla kalvoilla oli tyypillisesti korkeampi kasvunopeus. Havaittu kasvunopeus oli noin 0,5–0,85 Å/sykli. Poikkeus tähän oli kalvo, joka kasvatettiin AlN:n päälle, jonka kasvunopeus oli 0,35 Å/sykli. Paras resistiivisyys, joka plasman avulla saavutettiin oli 490 μΩcm. ToF-ERDA mittausten perusteella vety-plasmalla kasvatetuissa kalvoissa oli typpeä, jonka lähteeksi todettiin kantajakaasu. Yksikään kasvatetuista kalvoista ei ollut suprajohtava.

Lopputuloksena päädyttiin siihen, että ammoniakin pelkistyskyky ei ole riittävä, jotta pystyttäisiin kasvattamaan stoikiometrista NbN:ä. Lisäksi todettiin, että vedyn käyttö lisäpelkistimenä, samaan tapaan kuin sinkkiä on käytetty, vaatisi korkeammat lämpötilat toimiakseen. Suprajohtavien kalvojen kasvatuksen pitäisi olla mahdollista plasman avulla, kunhan ALD-laitteseeen saadaan tehtyä muutos, jotta kaikki kantajakaasut olisivat argonia.

Avainsanat Atomikerroskasvatus, niobiumnitridi

Acknowledgements

First of all I would like to thank M.Sc. Maria Berdova whom I had the pleasure of working with and who got me started with this interesting project.

Then I would like to thank few persons who have participated in the thin film characterization. I would like to thank M.Sc. Saima Ali and M.Sc. Sakari Sintonen from Aalto University for performing some of the XRR and GIXRD measurements, M.Sc. Jaakko Julin and Ph.D. Timo Sajavaara from University of Jyväskylä for performing ToF-ERDA measurements, M.Sc. Hannele Heikkinen from VTT for performing the wafer curvature measurements and M.Sc. Mikko Kiviranta from VTT for performing superconductivity measurements.

Finally I would like to thank D.Sc. Riikka Puurunen for giving guidance at the end of this work, Prof. Sami Franssila for giving the opportunity and guidance to complete this and whole MECHALD project group for support in this work.

This work was conducted within MECHALD project funded by TEKES (Finnish Funding Agency for Innovation).

Table of Contents

Acknowledgements 4

Definitions 7

1 Introduction 8

2 Thin film vacuum deposition methods 10

2.1 Physical vapor deposition 10

2.2 Chemical vapor deposition 10

2.3 Atomic layer deposition 11

2.3.1 Introduction 11

2.3.2 Principles 12

2.3.2.1 Thermal ALD 12

2.3.2.2 Plasma-enhanced ALD 15

3 Transition metal nitride thin films 18

3.1 Introduction 18

3.2 Sputtering of transition metal nitrides 20

3.3 CVD of transition metal nitrides 21

3.4 ALD of transition metal nitrides 22

3.4.1 Titanium nitride 23

3.4.1.1 Thermal processes 23

3.4.1.2 Plasma processes 27

3.4.2 Tantalum nitride 29

3.4.2.1 Thermal processes using $TaCl_5$ 29

3.4.2.2 Plasma processes using $TaCl_5$ 30

3.4.3 Niobium nitride 31

3.4.3.1 Thermal processes 31

3.4.3.2 Plasma processes 34

4 Experimental 36

4.1 ALD tool 36

4.2 Deposition parameters 38

4.3 Characterization 39

5 Results and discussion 43

5.1 Thermal depositions 43

5.1.1 Depositions with NH_3 43

5.1.2 Depositions with H_2 and NH_3 54

5.1.3 Summary of thermal depositions 55

5.2 Plasma depositions 55

5.2.1 Depositions with $Ar/H_2/N_2$ plasma 55

5.2.2 Depositions with Ar/H_2 plasma 57

5.2.3 Depositions with NH_3 plasma 59

5.2.4 Summary of plasma depositions 59

6 Conclusion and outlook 60

References 62

Appendix A: Compilation of deposited samples 71

Appendix B: Thickness and resistivity of samples 7-11 78

Appendix C: ToF-ERDA depth profiles for samples MS1-5 79

Definitions

Non-uniformity is used to describe how dissimilar specific value, e.g. thickness or sheet resistance, is across the substrate. It is given in percentage. Two common ways to calculate it is standard deviation as percentage or (maximum value – minimum value) / (2 x average) as percentage. The latter is used in this thesis. Typical values for ALD films are ca. 1 %.

Uniformity is opposite of non-uniformity. 100 % - non-uniformity.

Conformality describes how uniform film thickness is reproduced over the topography of a structured substrate. The higher the value the better the deposited film follows the topography. 100 % conformality is also called as conformal deposition.

Aspect ratio is defined as depth of a structure divided by its width. Structures with aspect ratio of ten or over are typically described as high aspect ratio.

Homogeneity is used to describe uniformity of film properties across substrate and film thickness.

Surface roughness or shortly roughness is a component of surface texture. It is typically calculated as arithmetic average, R_A, or root mean square, R_{RMS}, of vertical deviation from reference plane. Higher value means rougher surface. Typical values for ALD films are ca. 1 nm.

Pin-hole is nanoscale hole through the whole film thickness allowing substrate to be exposed directly to ambient. Pin-holes in thin intermediate layers may allow contact between top and bottom layers through the intermediate layer.

1 Introduction

Atomic layer deposition (ALD) has emerged as enabling thin film technology for numerous applications from microelectronics to jewelry over the past few decades [1] [2]. It features ability for sub nanometer thickness control of high quality pin-hole free films and in theory perfect conformality for the deposited film into high aspect ratio or 3D-features, which are becoming ever more significant as device dimensions shrink.

Transition metal nitrides are known for their hardness, chemical inertness, high melting temperature and electrical properties [3]. Transition metal nitride thin films are used as hard wear resistant coatings in tools and decorative applications, and in microelectronics as conducting barrier layers between silicon and conducting metals. Niobium nitride has been explored as barrier material, but it is best known for high superconductive transition temperature of up to 17.8 K.

Superconductive niobium nitride has so far been deposited mainly by reactive sputtering for superconductive applications like superconductive single-photon detector (SSPD) and kinetic inductance detector (KID) [4] [5]. ALD offers advantages like improved conformality, homogeneity and thickness control over sputtering and is raising interest as deposition method for superconductive thin films.

The aim of this thesis is to develop deposition process for niobium nitride for the new ALD reactor Picosun SUNALE™ R-200 Advanced and especially explore the plasma processes which have not been studied for NbN except from organometallic precursors. Additional goal for the process development was deposition of superconductive niobium nitride thin films. Process development was started from scratch as the only prior processes developed for the new tool were aluminum oxide and titanium nitride at the start of the work.

Literature survey is structured so that it first covers principles of major thin film technologies: sputtering, chemical vapor deposition (CVD) and ALD, with emphasis on ALD. After that general overview of transition metal nitride thin films is given mainly focusing on titanium, tantalum and niobium nitride thin films and short overview on deposition of these thin films by sputtering and CVD. More thorough overview is given on atomic layer deposition of titanium, tantalum and niobium nitride thin films by reviewing prior scientific literature.

Experimental part is divided into sections describing experimental methods; results and discussion; and finally conclusions and outlook. In experimental methods section first ALD reactor is described after which used deposition parameters and characterization methods are described. Results and discussion is divided into two main sections: depositions using thermal processes and depositions using plasma processes. In the final section conclusions are made based on the results and outlook is given.

2 Thin film vacuum deposition methods

2.1 Physical vapor deposition

Physical vapor deposition methods utilize physical means to transfer atoms from target to substrate. Common methods include evaporation and sputtering of which the latter is of interest in case of nitride films.

In sputtering target material is bombarded by energetic ions of inert gas, which is commonly argon. Energetic ions are created by plasma. Electric field is created between substrate and target with the former acting as anode and the latter as cathode. Ions are accelerated towards cathode, colliding with the target and ejecting atoms. These atoms are then deposited on the substrate. In reactive sputtering reactive atmosphere is present which enables deposition of nitrides, oxides and carbides. In case of nitrides this atmosphere usually consists of nitrogen and argon.

Vacuum vessel is usually pumped into a high vacuum prior to introducing deposition gases. During deposition vacuum vessel is under medium vacuum reducing the mean free path of atoms to smaller distance than the distance between the target and the substrate. This causes atoms to collide on their way to substrate, changing path and leading to enhanced step coverage. Substrate can be kept at room temperature during the deposition or it can be heated. Typical deposition rate for sputtered films range from 1 to 10 nm/s.

2.2 Chemical vapor deposition

Chemical vapor deposition (CVD) consists of a group of deposition methods which have in common that solid film is grown on substrate surface by chemical reaction from precursors that are in vapor phase. The precursors are fed into the reaction chamber where they chemically react at the surface or near the surface to form the film. Regarding the quality of the film it is important that the reaction occurs at the surface instead of in the gas phase. CVD methods usually require elevated temperatures to enable the chemical reactions or other ways like plasma-enhancement to introduce required energy. Typical deposition rate for CVD ranges from 0.1 to 10 nm/s.

Reaction types can be divided into four main types of reactions: thermal decomposition, reduction, exchange and coupled reactions [6].

In thermal decomposition reactions dissociation of gaseous precursor occurs resulting in solid and gaseous reaction products. Example of thermal dissociation reaction is decomposition of silane to deposit silicon:

$$SiH_4(g) \rightarrow Si(s) + 2H_2(g) \quad (1)$$

In reduction reactions at least two precursors are present. The other one acts as reducing agent. Common reducing agent in CVD processes is hydrogen. Example of reduction reaction is CVD deposition of tungsten from tungsten hexafluoride by reducing it with hydrogen.

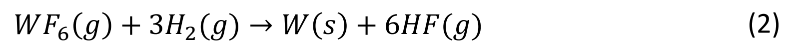

$$WF_6(g) + 3H_2(g) \rightarrow W(s) + 6HF(g) \quad (2)$$

Exchange reactions resemble reduction reactions, but no reduction takes place. Example of this type of reaction is deposition of zinc sulfide from zinc and hydrogen sulfide.

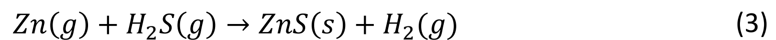

$$Zn(g) + H_2S(g) \rightarrow ZnS(s) + H_2(g) \quad (3)$$

Coupled reaction combines two different types of reactions. For example CVD deposition of titanium nitride from titanium tetrachloride, ammonia and hydrogen combines reduction and exchange reaction.

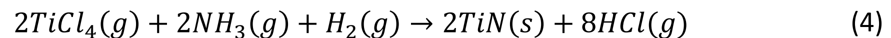

$$2TiCl_4(g) + 2NH_3(g) + H_2(g) \rightarrow 2TiN(s) + 8HCl(g) \quad (4)$$

Common CVD methods include Low-Pressure CVD (LPCVD), which operates at sub atmospheric pressures and is used commonly for deposition of stoichiometric Si_3N_4; Plasma-Enhanced CVD (PECVD), which is able to deposit films at lower temperatures; Metal-Organic CVD (MOCVD), which utilizes metal-organic precursors; and ALD, which is based on sequential pulsing of precursors forming single saturated layer at a time on top of a substrate separated by purge steps of inert gas.

2.3 Atomic layer deposition

2.3.1 Introduction

Atomic layer deposition has emerged as an enabling technology for a wide range of applications [1]. Semiconductor industries adopted ALD in 1990s and by the end of the decade it had become key enabling technology for them [1]. Since then ALD has found ever increasing number of applications utilizing the key properties of ALD films: high quality, conformal films with precise thickness and composition control [1] [7] [8].

Principle of ALD was first discovered in Soviet Union by Prof. S. I. Kol'tsov and Prof. V. B. Aleskovskii already in early 1960s under the name of Molecular Layering [9] [10]. However, knowledge of it did not become widespread [9] [10]. Without knowledge of work conducted in Soviet Union, Dr. Tuomo Suntola and co-workers developed ALD technology under name of Atomic Layer Epitaxy in 1970s to produce high quality ZnS thin films for electroluminescent flat panel displays. It became the first commercial application for ALD [9] [10]. The most common and best known ALD material is aluminum oxide deposited from $Al(CH_3)_3$ and water. Originally ALD Al_2O_3 answered the need for thin conformal insulating layer with good dielectric strength for magnetic heads. This was the second commercial application of ALD [11].

First deposition of nitride films by ALD was published in 1988 when nitride films of titanium, niobium, tantalum and molybdenum were grown in Laboratory of Inorganic and Analytical Chemistry at Helsinki University of Technology by Hiltunen et al. [12]. TiN from $TiCl_4$ and NH_3 has since become the most commonly used ALD nitride.

2.3.2 Principles

2.3.2.1 Thermal ALD

Atomic layer deposition is based on irreversible self-saturating gas-solid half-reactions taking place at substrate surface. In order to initiate a reaction on a substrate it has to have suitable surface groups illustrated as empty circles in Figure 1. During the first precursor pulse (Step 1) reactant A reacts with the surface until all of the available surface sites have been used. In the next step (Step 2) chamber is flushed with inert gas that carries away any remaining precursor and reaction by-products. In the subsequent step (Step 3) reactant B is fed into the chamber reacting with the surface until saturation, followed again by purge step with inert gas (Step 4). These four steps are a minimum for one ALD cycle. By repeating the cycle film thickness is increased. This cyclic deposition has led to commonly describing growth rate in ALD as thickness per cycle, hence growth per cycle (GPC), instead of typically used thickness per time unit. Typical growth rates for ALD range from 0.2 to 1.5 Å/cycle and are dependent on the deposited material and used precursors. This leads to growth rate of few nm/min depending on ALD tool. Longer pulsing and purging times are required for larger reaction chamber resulting in increased cycle time and decreased growth rate per minute.

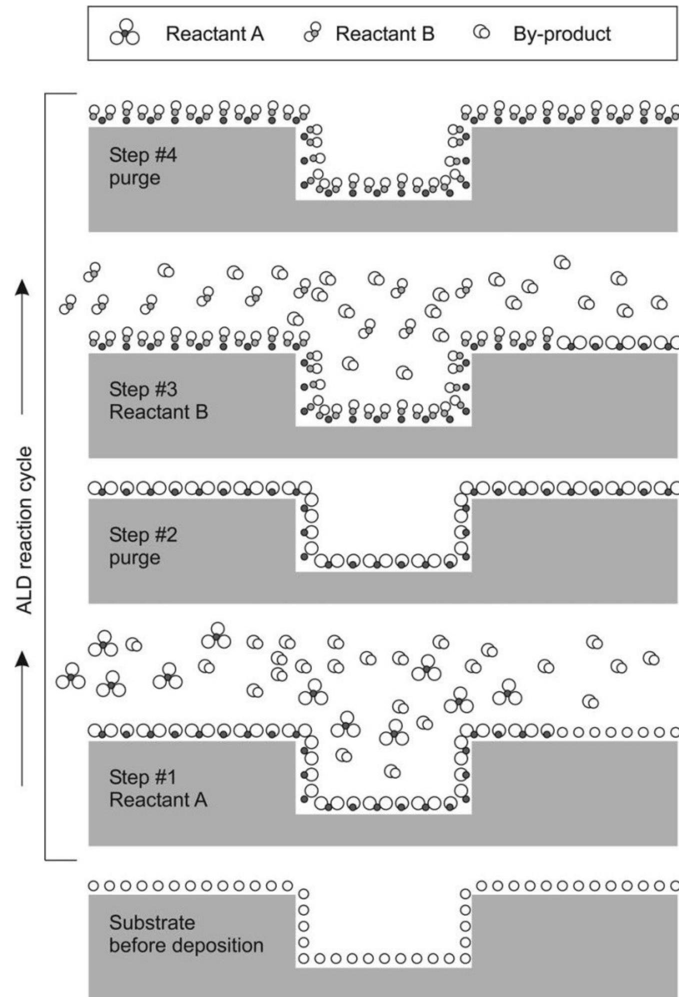

Figure 1: Schematic image of one ALD cycle consisting of four steps: Step 1 Reactant A pulse, Step 2 purge, Step 3 Reactant B pulse and Step 4 purge. Picture from Puurunen, R. L., Journal of Applied Physics, vol. 97, 2005 [13].

Due to the irreversible and self-saturating half-reactions ALD is described being conformal and uniform over large areas and complex shapes. This enables also thickness and composition control at sub-nm scale and creation of complex nanolaminate and mixed structures. On the other hand, due to the very same reasons, ALD is also slow compared to other deposition methods.

Another feature of ALD is weak temperature dependence of growth per cycle within ALD window shown in Figure 2 [8]. ALD window, Suntola's original concept, is described as the temperature range where irreversible and self-saturating half-reactions take place and thus fulfilling requirements for ALD-like growth [14]. Outside of ALD window GPC can increase due to decomposition and adsorption of precursor at high temperatures resulting in similar deposition as in unimolecular CVD. GPC can also increase by condensation of precursor on

substrate at low temperatures. Decrease in GPC can result from incomplete reactions at too low temperatures or by desorption of surface species at high temperatures [15]. Within the ALD window GPC can vary slightly with temperature as depicted in Figure 3 [13]. GPC can be decreased as in Figure 3 (a) if number of active surface sites or number of chemisorbed species decreases when temperature increases. GPC can stay constant as in (b) if steric hindrance is limiting the amount chemisorbed species. GPC can increase as in (c) when higher temperature enables new reaction paths. GPC can also first increase when new reaction paths are enabled and then decrease due to decreasing number of active surface sites as in (d).

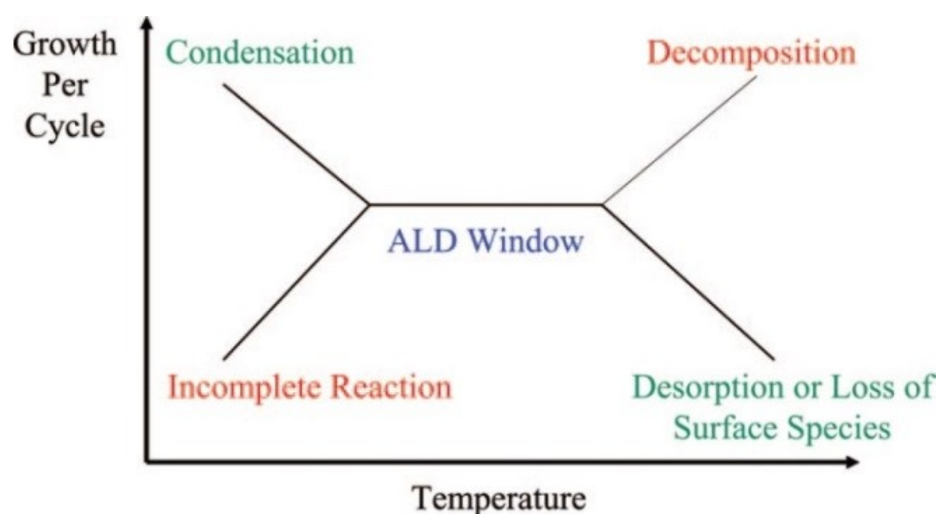

Figure 2: Schematic depiction of ALD window. Outside ALD window condensation and decomposition of precursor leads to increase while incomplete reaction and desorption or loss of surface species lead to decrease in growth per cycle. Picture from George, S. M., Chemical Reviews, vol. 110, 2010 [15].

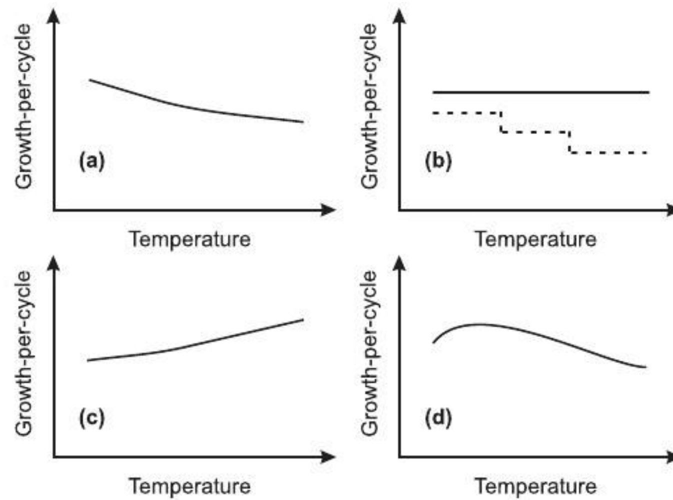

Figure 3: Schematic illustration how GPC may vary within ALD window from Puurunen, R. L., Journal of Applied Physics, vol. 97, 2005 [13].

2.3.2.2Plasma-enhanced ALD

Plasma-enhanced ALD offers several advantages over thermal ALD. High reactivity of plasma species allows higher freedom in processing conditions and new ways to affect material properties. Plasma enhancement also enables use of less reactive precursors that cannot be used in thermal processes. Plasma species bring increased energy to surface processes and PEALD films grown at same temperature as thermal films are commonly found to be of higher quality. This can mean increased film density, lower impurity content and better electronic properties [16]. Also growth per cycle is typically higher in PEALD processes compared to thermal processes.

Different types of plasma enhancement can be distinguished for atomic layer deposition as shown in Figure 4 depending on what kind of plasma is used. In direct plasma as in Figure 4 (a) substrate holder acts as the other cathode and the substrate is exposed directly to all the plasma species. In remote plasma, Figure 4 (b), plasma species are generated away from the substrate decreasing the damage caused by plasma on the substrate. In remote plasma, Figure 4 (c), the plasma is generated remotely and radicals flow to the substrate. This removes the damage caused by energetic ions on the substrate, but at the same time due to the long distance the plasma radicals have to travel to reach the surface it reduces the flux of radicals significantly due to recombination of plasma species.

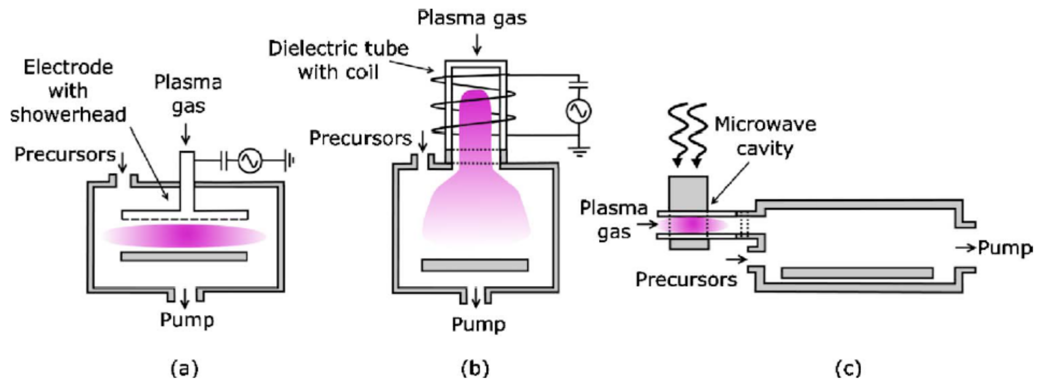

Figure 4: Different types of PEALD: (a) direct plasma, (b) remote plasma and (c) radical enhanced. From Heil et al., Journal of Vacuum Science & Technology A, vol. 25, 2007 [17].

Plasma enhancement comes with downsides also. Although GPC is higher compared to thermal processes, cycle times are also typically longer depending on the reactor type. Especially remote plasma and radical enhanced reactors are slower compared to thermal reactors. Another issue is compromised conformality in high-aspect ratio and 3D-structures due to recombination of plasma species [16]. Recombination probability depends on chosen plasma type and substrate surface. Overview of recombination probabilities on different surfaces is given on Table 1. Conformality can be improved by extending plasma exposure time and conformal deposition into structures with aspect ratio of 10 is still within reasonable limits [16]. Another limitation is plasma-induced damage. This can be due to reactive species in plasma oxidizing or nitridizing substrate surface layers, or energetic ions bombarding the substrate breaking bonds, displacing atoms and causing charge accumulation in dielectric layers, or plasma radiation degrading film properties [16].

Table 1: Overview of recombination loss probabilities of H, N and O radicals on different substrates adapted from Profijt et al., Journal of Vacuum Science and Technology A, 29, 2011 [16].

Radical	Surface	Recombination loss probability	Radical	Surface	Recombination loss probability
H	SiO_2	0.0004±0.00003	N	SiO_2	0.0003±0.0002
	Al_2O_3	0.0018±0.0003		Stainless steel	0.0063
	Pyrex	0.0058±0.0018		Si	0.0016
	Stainless steel	0.032±0.015		Al	0.0018
	Ti	0.35	O	SiO_2	0.0002±0.0001
	Al	0.29		Pyrex	0.000045
	Ni	0.20±0.09		Al_2O_3	0.0021
	Cu	0.14		ZnO	0.00044
	Au	0.15±0.05		Fe_2O_3	0.0052
	Pd	0.07±0.015		CuO	0.043
	Pt	0.03		Stainless steel	0.070±0.009

3 Transition metal nitride thin films

3.1 Introduction

Transition metal nitrides are known for their hardness, chemical inertness, high melting point and electrical properties [3]. TiN is commonly used as wear resistant coatings and due to attractive golden color also as a decorative coating. Electrical properties of TiN and TaN are exploited in microelectronics where they are used as diffusion barriers between metal conductors and silicon. In this context they are commonly referred to as barrier metals due to their electrical conductivity even though they are ceramics. In Table 2 resistivity of transition metal nitrides is compared to appropriate metal. NbN has found applications in superconductive electronics due to its relatively high transition temperature of about 15K for polycrystalline films and up to 17,8K for epitaxial films [18].

Table 2: Electrical resistivity of transition metals and transition metal nitrides from Koutsokeras, L., Doctoral Thesis [19].

	Electrical resistivity at 25°C (μΩcm)	
Element	Metal	Nitride
Ti	39	25
Zr	41.1	21
Hf	30	56.5
V	20.1	85
Nb	15.2	58
Ta	12.4-14.7	135-250
Cr	20.8	79
Mo	5.5	19.8
W	5.4	9

In metallic films the electrical resistivity is inversely proportional to electron mean free path and the conduction electron density [20]. Electron mean free path is affected by scattering of conduction electrons from surface due to small film thickness, uneven or rough surfaces,

grain boundaries and impurities [21]. When the thickness of the film is over two times the mean free path of the conduction electrons, increase in resistivity is no longer dominated by scattering from surfaces [21].

Transition metals can be found in multiple oxidation states. Titanium can be found in oxidation states ranging from -1 to +4, tantalum and niobium from -1 to +5. This leads to formation of phases with different structures. Titanium nitride can be found as Ti_2N and TiN while tantalum and niobium nitride have more possible variants as is shown in Table 3 for NbN. In addition to the presented stoichiometric phases, existence of these phases as nonstoichiometric phases is possible. From the proposed titanium-nitrogen phase diagram (Figure 5) it is possible to see the existence of cubic TiN phase with composition ranging from almost 2:1 to slightly over stoichiometric film. However, phase with higher nitrogen to metal ratio is not observed and stability of cubic TiN can extend further into nitrogen rich side. The structure of binary transition metal nitrides can be described as defect structure with existence of vacancies and varying metal to nonmetal ratios. Properties of the transition metal nitrides depend on vacancy concentrations and metal to nonmetal ratio [3].

Table 3: Phases of niobium nitride and corresponding structure data from Terao, N., Journal of the Less-Common Metals, vol. 23, 1971 [22].

NbNx phase	Structure
Nb_2N	Hexagonal
Nb_4N_3	Tetragonal
NbN	Cubic
NbN	Hexagonal
Nb_5N_6	Hexagonal
Nb_4N_5	Tetragonal

The most interesting of these phases in case of TiN, TaN and NbN is the cubic phase. This phase is the best conducting phase for all of the mentioned metal nitrides and the only phase that has superconductive transition temperature [3] [23]. Structure of the cubic phase is B1, same as observed for NaCl and hence called rock salt structure.

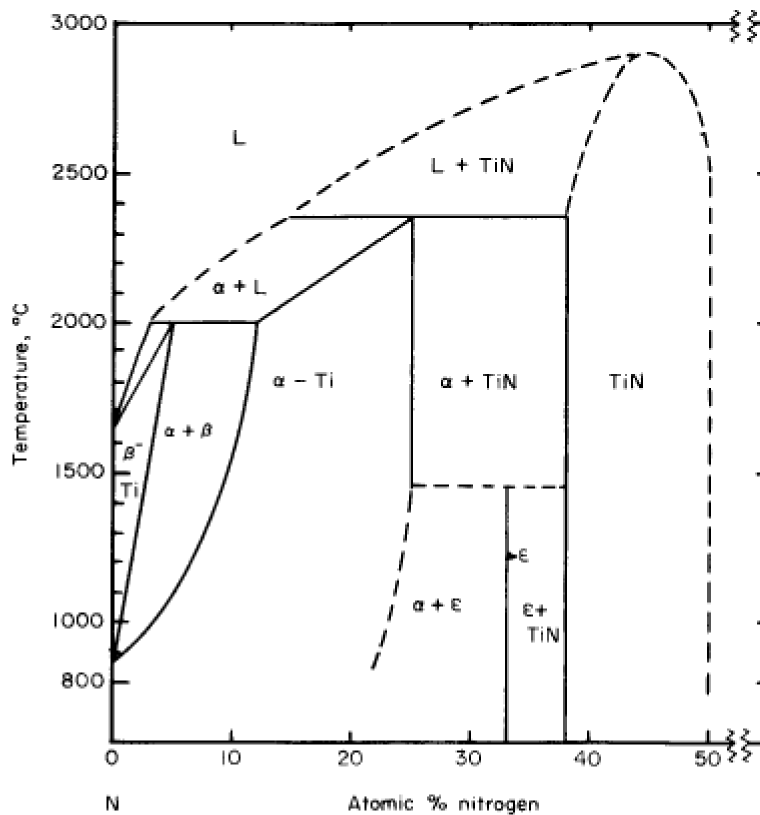

Figure 5: Proposed titanium-nitrogen phase diagram from Toth, L. E., Transition Metal Carbides and Nitrides, 1971 [3].

3.2 Sputtering of transition metal nitrides

Sputtering has often been the choice to deposit transition metal nitride thin films. Adjusting partial pressure of nitrogen inside reactor allows control of film composition allowing desired phase to be easily obtained. The films are generally free of impurities as long as chamber atmosphere and target are free of impurities. Resulting films have shown low resistivity and even epitaxial films have been deposited [24, 25] [26]. Although sputtering is often described as room temperature process, best quality films with sputtering are also often done at elevated temperatures.

Epitaxial NbN films have shown resistivity in the range of 30–70 μΩcm for films with superconducting transition temperature above 16 K [24, 25], while for polycrystalline films resistivity is higher around 150 μΩcm [27]. Polycrystalline TiN films have shown resistivity as low as 11 μΩcm [28] while the typical range varies from bulk resistivity of 24 to 40 μΩcm [29] [30]. Epitaxial TiN films have shown resistivity of 16.6 μΩcm [26].

Sputtering is used to deposit metallic layers of Nb and NbN for superconductive electronics [18]. It, however, has limitations in conformality.

3.3 CVD of transition metal nitrides

Conventional CVD of transition metal nitrides using metal halides is limited to high deposition temperatures required. It offers improvements in conformality over PVD methods. Nitride films from metal halides using molecular hydrogen and nitrogen require temperatures above 1000 °C as is visible from thermodynamic calculations for TiN in Figure 6 [31]. By using ammonia lower deposition temperatures are possible, but the required temperatures are over 500 °C [31]. TaN from $TaCl_5$ with NH_3 requires temperatures above 900 °C [32]. These temperatures are too high for semiconductor processing which is why CVD has been mainly used for wear-resistant and decorative coatings on substrates that tolerate the temperature.

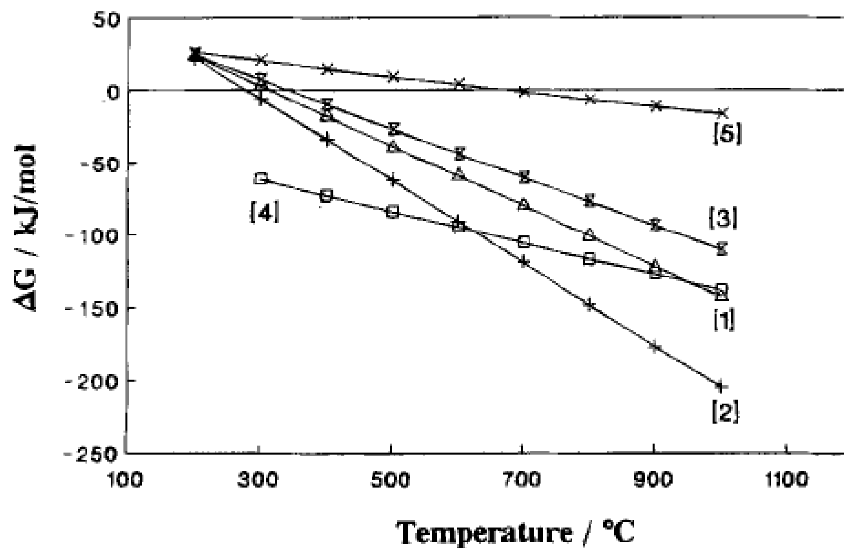

Figure 6: ΔG vs. temperature for formation of 1 mol of TiN according to reactions:

[1] $TiCl_4(g) + \frac{4}{3}NH_3(g) \rightarrow TiN(s) + 4HCl(g) + \frac{1}{6}N_2(g)$

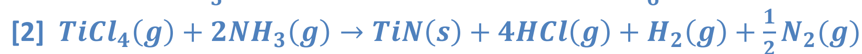
[2] $TiCl_4(g) + 2NH_3(g) \rightarrow TiN(s) + 4HCl(g) + H_2(g) + \frac{1}{2}N_2(g)$

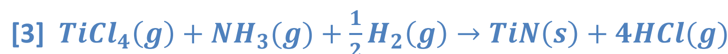
[3] $TiCl_4(g) + NH_3(g) + \frac{1}{2}H_2(g) \rightarrow TiN(s) + 4HCl(g)$

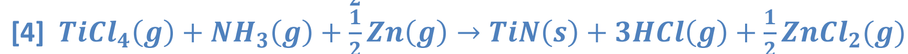
[4] $TiCl_4(g) + NH_3(g) + \frac{1}{2}Zn(g) \rightarrow TiN(s) + 3HCl(g) + \frac{1}{2}ZnCl_2(g)$

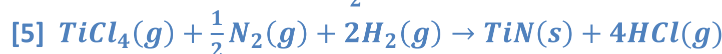
[5] $TiCl_4(g) + \frac{1}{2}N_2(g) + 2H_2(g) \rightarrow TiN(s) + 4HCl(g)$

From Ritala et al., Journal of Electrochemical Society, vol. 142, 1995 [33].

Typical resistivity of CVD TiN films is in the range of 200 to 6000 µΩcm which is higher than typically observed for reactively sputtered films [31]. CVD processes using $NbCl_5$, NH_3 and H_2 have produced superconductive NbN films but deposition temperatures have been above 900°C [34].

MOCVD has been used to reduce deposition temperature for nitride deposition, but the resistivity has been high, for TaN >900 µΩcm at 650 °C, and the quality of the films in terms of impurities and density was poor [35, p. 429]. Another aspect for reducing temperature has been PECVD where lowest resistivity value obtained for TaN films is 150 µΩcm using $TaBr_5$ and H_2/N_2 plasma at 450 °C [36].

3.4 ALD of transition metal nitrides

Chloride precursors are commonly used for ALD of transition metal nitrides and oxides. Metals in the chloride precursors are typically in higher oxidation state than in the film that is grown and they have to be reduced. Typical chloride precursor used for titanium is $TiCl_4$ where titanium is in +IV oxidation state while precursors of choice for tantalum and niobium are $TaCl_5$ and $NbCl_5$ respectively. For niobium and tantalum nitride films metal from the precursor needs to be reduced from +V to +III to obtain film with 1:1 composition.

Half-reactions for titanium nitride using ammonia can be represented as

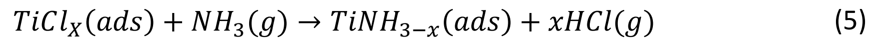

$$TiCl_X(ads) + NH_3(g) \rightarrow TiNH_{3-x}(ads) + xHCl(g) \quad (5)$$

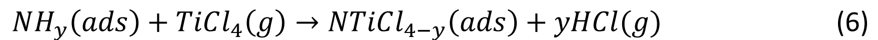

$$NH_y(ads) + TiCl_4(g) \rightarrow NTiCl_{4-y}(ads) + yHCl(g) \quad (6)$$

where x<4 and y<3. Overall reaction would be

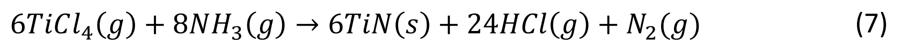

$$6TiCl_4(g) + 8NH_3(g) \rightarrow 6TiN(s) + 24HCl(g) + N_2(g) \quad (7)$$

This includes also the most likely oxidation byproduct N_2 which, however, has not been experimentally detected [37]. Another alternative for the reaction is also

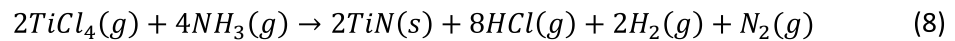

$$2TiCl_4(g) + 4NH_3(g) \rightarrow 2TiN(s) + 8HCl(g) + 2H_2(g) + N_2(g) \quad (8)$$

At lower temperatures reduction of titanium may not fully occur, giving TiNCl as a product instead according to [37]

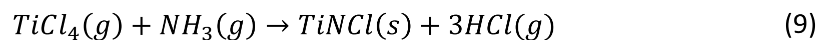

$$TiCl_4(g) + NH_3(g) \rightarrow TiNCl(s) + 3HCl(g) \quad (9)$$

This would explain the increase of chlorine impurities with decreasing temperature. Another source for chlorine impurities may be formation of ammonium chloride during

ammonia pulse. Decomposition of ammonium chloride is probable at higher temperatures (ΔG negative above 370 °C) [38].

Using zinc as reducing agent changes the overall reaction equation to

$$2TiN_4(g) + Zn(g) + 2NH_3(g) \rightarrow 2TiN(s) + ZnCl_2(g) + 3HCl(g) \quad (10)$$

However, the use of zinc limits suitable deposition temperatures to above 400°C due to its low vapor pressure. In addition, concerns of zinc contamination causing severe problems have prohibited its use in microelectronics [11].

Thermodynamically favorable reactions can be seen from Figure 6 where change in Gibb's free energy, ΔG, is presented for different TiN deposition reactions. From these we can see how the reactions with molecular hydrogen and ammonia are not thermodynamically favorable compared to reactions without molecular hydrogen. Also addition of zinc into the reaction makes reactions more favorable at lower temperatures. However, these values only take into account overall reactions happening according to reactions presented as in CVD and do not reflect the real ALD process involving formation of surface species.

For niobium and tantalum nitride the overall reaction using M for niobium or tantalum would look like

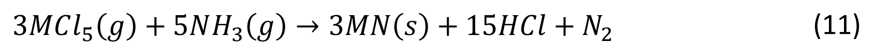

$$3MCl_5(g) + 5NH_3(g) \rightarrow 3MN(s) + 15HCl + N_2 \quad (11)$$

In plasma processes utilizing H_2/N_2-plasma overall reaction would be

$$MCl_5(g) + 5H(g) + N(g) \rightarrow MN(s) + 5HCl(g)$$

It is also possible to introduce the plasmas separately as an ABC process.

3.4.1 Titanium nitride

3.4.1.1 Thermal processes

Depositions with $TiCl_4$ and NH_3

In the first published TiN deposition by Hiltunen et al. [12] two cubic δ-TiNx films with different stoichiometry at 500 °C were deposited on soda lime glass. Since then deposition temperatures have ranged from 300 to 550 °C [39] [40] [41]. The first film by Hiltunen et al. had 40 at% nitrogen and was golden yellow with resistivity of 240 μΩcm and second one had 50 at% nitrogen being dark violet and having resistivity of 360 μΩcm. Growth rate was

0.02–0.03 Å/cycle. This is thought to be the typical growth rate although lower rate of 0.17 Å/cycle has been observed by Ahn et al. [42] and Ritala et al. [33] while higher rates of 0.4 and 0.6 Å/cycle has been observed by Jeon et al. [43] and Kim et al. [44] respectively. Dependence of growth rate on deposition temperature has been described from small to nonexistent [39] [40] [42] [44].

Thermal ALD TiN films are stoichiometric or really close to stoichiometric, and polycrystalline. Chlorine impurities increase with decreasing temperature. Above 400 °C chlorine content is commonly observed to be under 1 at% [43] [45] [44] [46]. Cheng and Lee [40] had slightly higher concentration, 2 at% at 450 °C. They however observed that using 6-step ALD cycle introducing pump-down steps before purge steps decreased chlorine contamination significantly. At 300 °C they had 7.7 at% of chlorine with 4-step process, but only 2.3 at% with 6-step process. Chlorine concentration went below detection limit of 1 at% at 350 °C with 6-step process and with 4-step process at 500°C.

Density increase with increasing temperature has been observed [43]. Jeon et al. [43] observed increase in density from 4.2 to 4.7 to 4.85 g/cm^3 with decreasing chlorine content from 2.5 to 0.5 to 0.3 at% with deposition temperature increasing from 350 to 400 to 450 °C. Ahn et al. [42] however suggested that the main cause for the increase in density would not be caused by decrease in impurity content as their chlorine content remained below 2 at% for every deposition temperature. Instead they observed a change in the preferred orientation from [100] to the most densely packed [111] at higher temperatures leading to increase in density. However, for Jeon et al. no preferred orientation was detectable although [111] peak appeared at higher temperatures.

Titanium nitride surface oxidizes when exposed to air. Kim et al. [44] noted that reaction

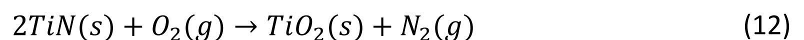

$$2TiN(s) + O_2(g) \rightarrow TiO_2(s) + N_2(g) \quad (12)$$

is thermodynamically favorable and surface oxidation is commonly observed [43] [45] [44] [39]. Langereis et al. [20] observed increase in resistivity for ex situ measurements compared to in situ and related this to post-deposition oxidation. The amount of oxygen in the film due to post-deposition oxidation is dependent on the deposition temperature and the effect is reflected on difference in in situ and ex situ resistivity as shown in Figure 7. It seems that films deposited at lower temperatures are more prone to post-deposition oxidation which might be related to less dense microstructure. However, the data in Figure

6 by Langereis et al. [20] might be slightly misleading, as the thickness of the films is not exactly the same, but the thickness of the film deposited at 100 and 200 °C is comparable being 10.2 and 10.7 nm respectively while the film deposited at 400 °C is 23 nm thick.

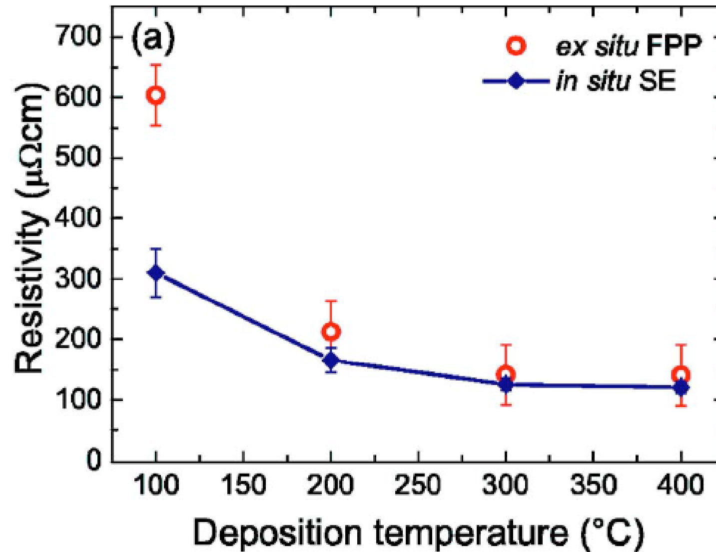

Figure 7: Resistivity measured in situ with spectroscopic ellipsometer and ex situ by four point probe as a function of deposition temperature from Langereis et al., Journal of Applied Physics, 100, 2006 [28].

Growth mechanism of ALD TiN was investigated by Choi et al. [41] at 550 °C on three different dielectrics: thermal SiO_2, HfO_2 and $HfSiO_x$. They observed that TiN growth starts as islands and density of islands depends on the substrate. Lowest density of islands after five cycles was observed on thermal SiO_2 while on HfO_2 it was densest. The island density combined with total reflection X-ray Fluorescence (TXRF) data, where lower reflection angle of titanium peak corresponding to lower mass density or rougher surface, was observed for TiN on SiO_2. This suggested change in growth mechanism from more three-dimensional on thermal SiO_2 to more two-dimensional on HfO_2. This initial growth is also affecting film coalescence, which was achieved after deposition of 2.4 nm layer on SiO_2 while only 0.6 nm on HfO_2. Initial growth has also influence on the final grain sizes where grain size on SiO_2 was larger.

Best resistivities obtained for TiN films grown with NH_3 is 72 μΩcm obtained by Ahn et al. [42] for film deposited at 500 °C and 75 μΩcm obtained by Jeon et al. [43] at 450 °C. Ahn et al. [42] also determined that about 30 nm film thickness is required for film resistivity to become independent on film thickness. Ritala et al. [33] noticed saturation of resistivity

only after 100 nm for films grown with zinc, but then again thinner films had higher oxygen content than thicker films. These values are higher than what is obtained for PEALD TiN films where Langereis et al. [20] determined in situ that after 15 nm effect of film thickness on resistivity is weak as shown in Figure 8 (a). They determined that the conduction electron density saturates and starts to slowly decrease after 15 nm and electron mean free path increases, but at reduced rate, after 15 nm with increasing thickness as shown in Figure 8 (b). However, electron mean free path is small (0.65 nm in the thinnest film) compared to film thickness (2 nm in the thinnest film) and thus according to Lacy [21] other scattering effects are the main reason for decrease in resistivity rather than scattering due to thickness. This leads to conclusion that scattering from grain boundaries, uneven or rough surface or impurities are more pronounced in thinner films. Langereis et al. [20] attributed the decrease in mean free path solely on the decrease in thickness.

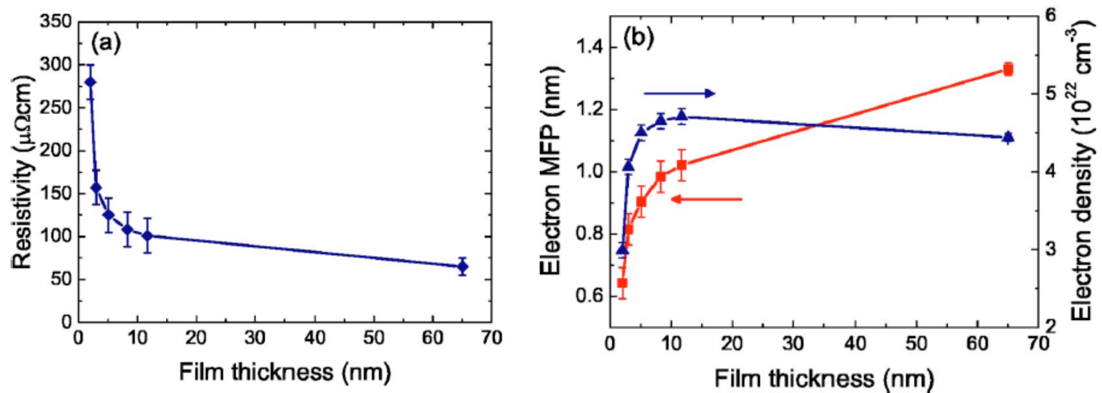

Figure 8: (a) Effect of thickness on resistivity for TiN film grown by PEALD and (b) thickness dependence of factors affecting resistivity: electron mean free path and conduction electron density from Langereis et al., Journal of Applied Physics, vol. 100, 2006 [20].

Commonly observed trend for resistivity is to decrease with increasing temperature for example Jeon et al. [43] observed decrease in resistivity from 350 to 75 μΩcm when temperature was increased from 350 to 450 °C. Langereis et al. [20] observed decrease in electron mean free path in their in situ spectroscopic ellipsometry studies as deposition temperature decreased while conduction electron density remained practically constant. Decrease in mean free path can be related to increase in impurity concentration, especially chlorine, with decreasing temperature which increases electron scattering. Mean free path is influenced also by grain size, which tends to be larger at higher temperature although Langereis et al. [20] concluded that electron mean free path is not limited by the grain size. Another factor affecting the measurements is the variation of thickness as the films were

deposited with same amount of cycles leading to film deposited at 100 °C being half of the thickness of the film deposited at 400 °C.

Effect of intermediate zinc pulses

Small decrease in growth rate was observed with decreasing temperature by Ritala et al [33]. However, they did not observe big difference in growth rate between TiN films grown with or without zinc at 500 °C. The biggest difference in the films grown without zinc to films with zinc was change in preferred orientation in thicker films from [100] to [111] [33] [46]. Films grown with zinc also showed slightly bigger grain size than film grown without zinc which was observed as an increase of root mean square (rms) roughness from 5.2 nm to 7.9 nm measured by AFM [33]. Both of the films were oxygen contaminated uniformly through the film thickness of 120 nm, but the film grown without zinc had 15 at% oxygen compared with 2 at% in film grown with zinc [46]. Thinner films contained even higher percentages of oxygen and Ritala et al. [33] suggested that the source of oxygen would be post-deposition oxidation along grain boundaries. This would mean that structure of films grown with or without zinc would have to account for difference in oxidation which seems unlikely. Ritala et al. [46] also comment on this that the difference in grain size is between the films is too small to explain solely the differences in the films oxygen content.

Resistivity of the film grown with zinc was 46 µΩcm and without zinc it was 270 µΩcm, both for films deposited at 500 °C [46]. Corresponding effective carrier concentrations and Hall mobilities are $3.4 \cdot 10^{22}$ cm^{-3} and 0.7 cm^2/Vs for films grown without zinc and $6.4 \cdot 10^{22}$ cm^{-3} and 2.1 cm^2/Vs for films with zinc. Increase in Hall mobilities is likely to be result from decrease in oxygen impurities and grain boundaries compared to film grown without zinc while reason for difference in carrier concentrations is likely related to impurity content [46]. Whether the reason for decrease in oxygen content and thus resistivity is due to intermediate zinc pulses is debatable. However, the resistivity obtained for film grown with zinc is higher than the best obtained in thermal processes with $TiCl_4$ and NH_3.

3.4.1.2Plasma processes

Depositions with $TiCl_4$ and H_2/N_2-plasma

With plasma enhancement the deposition temperatures for TiN have been reduced to as low as 100 °C. However, the films have high impurity content [47] [20]. Observed growth rates of around 0.4 Å/cycle at 300°C are higher than for thermal TiN [47] [17] [48] [49]. In

contrast to thermal depositions where growth rate was not affected significantly by the deposition temperature, in PEALD of TiN deposition temperature affects growth rate strongly. Langereis et al. [20] observed increase in growth rate from 0.26 to 0.62 Å/cycle when deposition temperature increased from 100 to 400 °C. Heil et al. [50] observed as high growth rates as 0.8 Å/cycle with extended plasma exposure times (>60s) at 400 °C.

With plasma enhancement chlorine impurity content can be reduced compared to thermal deposition especially at lower deposition temperatures. Langereis et al. [20] observed chlorine content of 0.3 at% at 400 °C which is similar to what has been observed for some thermal TiN films. However, already at 300 °C best thermal TiN films have 2.3 at% chloride impurities [40] while for Langereis et al. chlorine content is 0.4 at% at the same temperature and only 1 at% at 200 °C. Similar results have been observed by Kwon and Park [49] who observed increase in chlorine content from about 1 to 3 at % with deposition temperature decreasing from 300 to 200 °C. In addition to deposition temperature Elers et al. [51] reported that chlorine impurity content can be reduced by increasing plasma exposure time and by increasing plasma power. Heil et al. [47] [17] observed similar behavior with plasma exposure time.

Some amounts of hydrogen impurities are found in TiN films, but they are often left unreported because only few methods are able to detect them. Heil et al. [50] observed increase in hydrogen content in the film from 4 to 9 at% with increasing plasma exposure time from 5 to 60 s at 400 °C. At low temperatures 16 at% of hydrogen has been observed [47].

Controlling the N/Ti ratio is possible with plasma parameters [47] [49] [52]. Elers et al. [51] noticed that increasing plasma power from 100W to 400W changed the films from titanium rich, N/Ti ratio 0.93, to nitrogen rich, N/Ti ratio 1.1. N/Ti ratio can be controlled also with plasma exposure time [47] [49]. With increasing plasma exposure time from 5 to 60s, N/Ti ratio in the films changed from titanium rich 0.93 to nitrogen rich 1.15. Kwon and Park [49] reported also slight change in N/Ti ratio with change in partial flow ratio of H_2/N_2. At small ratios <0.1 films were nitrogen rich and at high ratios >1.8 titanium rich. The titanium rich films tended to have also high chlorine content (5 at%).

Density of PEALD TiN films increase with temperature and can be related partly to decrease in impurity content. Langereis et al. [20] observed increase in density from 3.7 to 4.9 g/cm^3

with increasing temperature from 100 to 400 °C. The value of 4.9 g/cm^3 is higher than the best reported one for thermal TiN (4.85 g/cm^3 [43]). Kwon and Park [49] observed even denser film having density of 5.03 g/cm^3. Bulk density of TiN is 5.21 g/cm^3 [23].

Similar nucleation behavior on thermal silicon oxide was observed by Langereis et al. [20] for PEALD TiN as Choi et al. [41] observed for thermal TiN. The growth initiates as islands and the nucleation delay is dependent on hydroxyl group density on the surface. As with thermal process film coalescence is observed after approximately 2 nm. The nucleation on hydrogen terminated silicon begins by formation of 2–3 nm interfacial silicon nitride layer on which the TiN film then nucleates and is hence the nucleation is slow.

Best resistivity obtained for PEALD TiN is 71 µΩcm at 400 °C [47], which is comparable to the best resistivities obtained for thermal TiN films at higher temperatures.

3.4.2 Tantalum nitride

3.4.2.1 Thermal processes using $TaCl_5$

Depositions with NH_3

The first published TaN deposition by ALD was published by Hiltunen et al. [12] in 1988. They deposited TaN from $TaCl_5$ and NH_3 on soda lime glass. Resulting films were either cubic TaN or tetragonal Ta_3N_5. Resistivity of the low resistivity cubic phase was 1190 µΩcm. Cubic TaN phase was found nitrogen rich with 56 at% nitrogen content.

Films deposited by Liu et al. [53] [54] at 300–390 °C were nitrogen rich and were determined to be dielectric Ta_3N_5 phase. Chlorine impurity content in the films was observed to be 1–2 at% and source was determined to be unbroken ligands in precursor molecules [53].

TaN films have been deposited between 200–500 °C on soda lime glass by Ritala et al. [55], and by Liu et al. [53] [54] on organosilicate glass and aromatic SiLK^{TM} at 300-390°C. Ritala et al. observed increasing GPC with increasing temperature from 0.12 Å/cycle at 200 °C and saturated to 0.20–0.25 Å/cycle above 300 °C. Chlorine impurity content increased with decreasing temperature. Liu et al. [53] determined that at deposition temperatures between 300–390 °C, source of chlorine impurities were unbroken ligands in precursor molecules. For Ritala et al. above 400 °C films have <1 at% chlorine content while already at

300 °C chlorine content was 5 at%. Liu et al. observed chlorine content of 1–2 at% for their films. The films were amorphous below 400 °C for Ritala et al. and crystalline orthorhombic Ta_3N_5 at or above 400 °C. The amorphous films exhibited resistivity above 200 Ωcm while crystalline Ta_3N_5 had resistivity of 0.5 Ωcm. Liu et al. only determined that their films were dielectric Ta_3N_5.

Oxygen impurity is determined mainly by the purity of the chemicals used, residual oxygen in reactor atmosphere and film exposure to ambient air. Ritala et al. [55] observed increase in oxygen content below 300 °C which is likely to originate from exposure to ambient air. Increase in the film oxidation for films grown at lower temperatures may originate from less dense structure which allows oxide to diffuse into the film more easily.

Effect of intermediate zinc pulses

Deposition of cubic TaN is possible with addition of intermediate zinc pulses between $TaCl_5$ and NH_3 pulses at temperatures above 400 °C [55]. Growth rate of films grown with intermediate Zn pulses, decrease with temperature from 0.2 Å/cycle at 400 °C to 0.15 Å/cycle at 500 °C as observed by Ritala et al. [55].

In contrast to films grown without zinc which had <1 at% of chlorine impurities above 400 °C , films grown with zinc had chlorine impurity content of 4.5 at% at 400 °C. Films grown at 400 °C exhibited also 0.5 at% of both zinc and hydrogen. Films grown at or above 450 °C were relatively clean except for 3–4 at% oxygen impurities which were independent of deposition temperature. Resistivity of cubic TaN films was approximately 900 µΩm regardless of deposition temperature.

3.4.2.2 Plasma processes using $TaCl_5$

Deposition of cubic TaN thin films by PEALD was realized by Kim et al. [56] using hydrogen-nitrogen plasma at temperatures between 100–400 °C. Plasma power was chosen so that atomic hydrogen was present, but nitrogen was just activated. Atomic hydrogen is able to extract chlorine from tantalum and reduce it, while activated nitrogen is incorporated into the film to form TaN.

Controlling N/Ta ratio is possible with PEALD [56]. At 300 °C Kim et al. [56] were able to control N/Ta ratio from 0.3 to 1.4 by varying N_2/H_2 partial pressure ratio from 0.001 to 1 as shown in Figure 9. Stoichiometric films were obtained at N_2/H_2 partial pressure ratio

between 0.025–0.035. Resistivity of cubic TaN films was 350–400 µΩcm, and higher with increasing nitrogen content. Plasma exposure time affected impurities, resistivity and growth rate. Growth rate saturates at 5 s after a peak at 2 s. With increasing plasma exposure time from 2 s to 5 s chlorine content decreased from 6 to 1 at%, hydrogen content increased from 4 to 10 at% and resistivity decreased from 600 to 350 µΩcm.

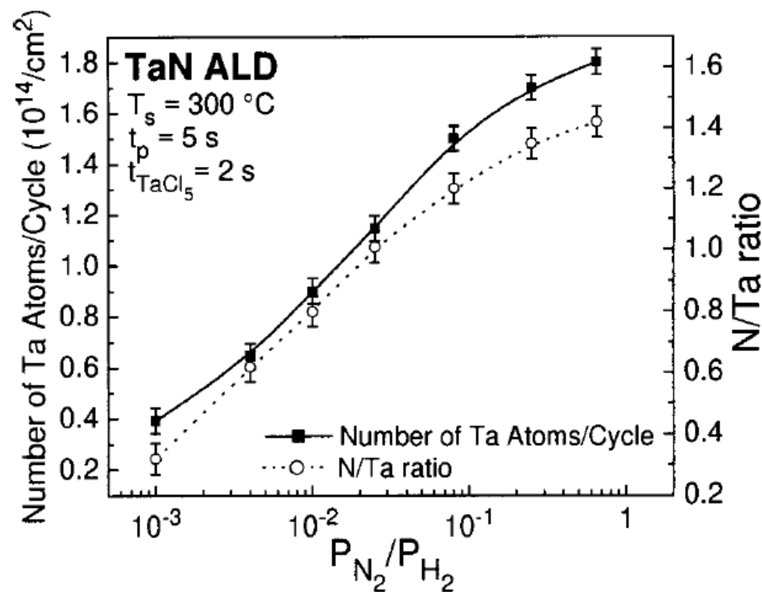

Figure 9: Effect of change in plasma partial pressure ratio in GPC and N/Ta ratio from Kim, et al., Journal of Applied Physics, 92, 2002 [56].

Effect of deposition temperature on composition and properties was investigated by Kim et al. [56] between 100–400 °C. Using N_2/H_2 partial pressure ratio of 0.025 the films were all crystalline cubic TaN. Growth rate increased strongly with increasing temperature while N/Ta ratio remained almost constant. Chlorine and hydrogen content decreased from 3 to <1 at% and 22 to 8 at% respectively with increasing temperature from 100 to 400 °C. Resistivity decreased only slightly from 420 to 350 µΩcm with increasing temperature.

3.4.3 Niobium nitride

3.4.3.1 Thermal processes

Depositions with $NbCl_5$ and NH_3

Deposition of NbN by ALD was published for the first time in 1988 by Hiltunen et al. [12] on soda lime glass substrate using alternating pulses of $NbCl_5$ and NH_3 at 500 °C. They observed growth of cubic δ-NbN with nitrogen content varying from 55–58 at%, but they

do not content of other elements. Room temperature resistivity was measured to be 200 µΩcm for 200 nm and 240 µΩcm for 90 nm thick films. Superconductive transition temperature was observed to exist at 10 K. This has been the only time when superconductive cubic δ-NbN has been grown thermally using just NH_3 as reducing agent. Since then all the films grown with $NbCl_5$ and NH_3 have produced more resistive phases [52] [46] [57] [58].

Superconductive transition temperature of ALD NbN from $NbCl_5$ has only been reported once after Hiltunen et al. [12] deposited their film in 1988. Proslier et al. [59] reported in a proceedings article transition temperature of 5 K for NbN grown with Zn.

Nb/N ratio of films grown by $NbCl_5$ and NH_3 has been less than 1 for all the films that has been reported. Alén et al. [58] observed Nb/N ratio of 0.8 between 250–500 °C regardless of deposition temperature. Similar Nb/N ratio was observed by Van Hoornick et al. [57]. Ritala et al. [46] observed even higher nitrogen content. For them Nb/N ratio was close to 0.7.

Chlorine content in the films is primarily determined by the deposition temperature. At 500 °C chlorine impurities are below 1 at% [52] [46] [58]. At lower temperatures chlorine level in the films increase. Between deposition temperatures of 400-500 °C it is possible to obtain relatively pure films containing only 1 at% of chlorine impurities [58]. Juppo et al. [60] observed considerable amount of chlorine in their films and increase in chlorine content from 15 at% to 24 at% when lowering deposition temperature from 400 °C to 300 °C. In comparison Alén et al. [58] observed only 8 at% at 250 °C. Amount of oxygen impurities is determined mainly by the purity of chemicals used, residual oxygen in reactor atmosphere and film exposure to ambient air. Alén et al. [58] observed 1 at% oxygen impurities in deposited films between 250–500 °C regardless of the deposition temperature.

Growth rate of films deposited by Juppo et al. were also strangely low being only 0.1 Å/cycle at both 300 and 400 °C. Alén et al. [58] observed increase in growth rate from 0.12 Å/cycle at 250 °C to 0.27 Å/cycle at 500 °C.

Resistivity of NbN films shows dependence of deposition temperature. While the best resistivity obtained for films grown without zinc is 550-600 µΩcm at 500 °C [58] [46] [52]

already at 400 °C resistivity is 750 μΩcm and at 300 °C 3000 μΩcm [58]. Increase in resistivity can be related partly to increase in chlorine content of the films.

Effect of intermediate zinc pulses

Cubic δ-NbN films have been grown thermally by introducing intermediate zinc pulse [52] [46] [61]. Zinc itself is able to reduce $NbCl_5$ all the way to metallic niobium [52]. Growth rate of NbN films grown at 500 °C with intermediate zinc pulses has been observed to be 0.18 Å/cycle while without zinc it is 0.25 Å/cycle [52] [46]. This decrease in GPC has been attributed to forming of Nb on which $NbCl_5$ is unable to chemisorb tightly [52]. This leads to decrease in active surface sites for the next cycle.

Chemical composition of NbN films grown with or without zinc does not differ significantly. For Ritala et al. [46] both films were nitrogen rich with N/Nb ratio of 1.5 with impurity content of less than 1 at%. The only observable change was slight decrease in oxygen content. They observed structural changes from XRD measurements where peaks were shifted slightly toward higher d-values (2.493->2.504 Å for (111)) for films grown with zinc. However the d-values for both films were clearly smaller than reference value 2.536 Å for cubic δ-NbN. Similar behavior was observed also by Elers et al. [52]. The biggest change in microstructure observed by Ritala et al. [46] was increase in grain size for films grown with zinc as observed from RMS roughness increase from 6.9 to 19 nm.

While NbN film grown with intermediate zinc pulses exhibit resistivity between 200–300 μΩcm, a film grown without zinc has resistivity between 550–600 μΩcm [52] [46]. For films grown with zinc trend of increased mobility and carrier concentration is observed. However, the measurement suffered from reproducibility issues and exact values could not be determined [46].

Use of 1,1-dimethylhydrazine as reducing agent

Use of 1,1-dimethylhydrazine (DMHy) as reducing agent for NbN growth instead of NH_3 was investigated by Juppo et al. [60]. The reason to use DMHy instead of NH_3 is the higher reactivity of DMHy. They observed decrease in chlorine content of the film from 15 at% to 5 at% compared to film grown with NH_3 at the same temperature. Also the growth rate was comparable to those grown at 500 °C. Determination of the phase was not made, but from the resistivity of >10000 μΩcm it would seem that it is not cubic. However, the film contained high amount of impurities that increase resistivity. No significant improvements

were observed from use of DMHy according Juppo et al. and comparison to films deposited by others is difficult due to poor quality of the films in the study (high impurity content in both DMHy films and reference NH_3 and strangely low GPC in reference films).

3.4.3.2 Plasma processes

NbN by plasma processes has been realized only with organometallic precursors aiming to eliminate chlorine impurities. Hinz et al. [62] used tert-butylimido-tris(ethylmethylamido)-niobium (TBTMEN) and hydrogen or hydrogen–nitrogen plasma at deposition temperatures between 200–350 °C to deposit NbN films while Ziegler et al. [63] used tert-butylimido-tris(diethylamido)-niobium (TBTDEN) and hydrogen plasma at temperatures between 200–400 °C. They observed growth rate of 0.62–0.64 Å/cycle which is over twice that of thermal NbN from $NbCl_5$ and NH_3 and over three times that of thermal NbN grown with help of zinc.

In comparison to NbN films grown from $NbCl_5$ which had Nb/N ratio below 1, films grown by Ziegler et al. have Nb/N ratio 1.15. In addition Hinz et al. were able to control nitrogen content of the films by adjusting partial pressure ratio of hydrogen–nitrogen plasma. Films deposited with just hydrogen plasma had Nb/N ratio of 0.8. When nitrogen was introduced into the plasma mixture nitrogen content in the films increased. Hinz et al. observed that 2 % concentration of nitrogen in plasma mixture produced NbN with 1:1 ratio and 10 % of nitrogen in plasma produced Nb/N ratio of 0.83. This ratio calculated by Hinz et al. assumes that part of the Nb is bound by oxygen as NbO_2.

Superconductive films with transition temperature of 10.2 K were obtained by Ziegler et al. while having 11 at% of oxygen as impurity. Films grown by Hinz et al. also contained high level of oxygen impurities. As the precursors do not contain oxygen, all the oxygen comes from reactor atmosphere or from exposure to air. Ziegler et al. does not mention anything about carbon content in the films and Hinz et al. claims that their films were carbon-free although some residual carbon is usually expected from organometallic precursors.

Resistivity of NbN films is affected by plasma parameters. Hinz et al. showed that lower plasma pressure resulted in decrease in resistivity and this was confirmed by Ziegler et al. Also extended plasma exposure time as shown in Figure 4 resulted in decrease in resistivity even after saturated growth [62] [63]. This effect saturates when plasma exposure time is further increased. Lowest resistivity obtained by Ziegler et al. [63] was 250 µΩcm at 400 °C which is comparable to thermal NbN films deposited at 500 °C with zinc even though the

films had high oxygen content. At lower temperatures resistivity increases, but even at 200 °C resistivity is as low as 800 μΩcm. All the films deposited between 200–400 °C by Ziegler et al. were superconducting. Transition temperatures ranged from 10.2 K at 400 °C to 4.5 K at 200 °C. Transition temperature tends to increase with decreasing room temperature resistivity. However, the lowest room temperature resistivity and the highest transition temperature do not necessarily coincide as is visible in Figure 10 and 11. Lowest resistivity Ziegler et al. obtained was with 30 s plasma exposure and highest transition temperature of 10.2 K with 85 s plasma exposure. Resistivity with 85 s plasma exposure was 350 μΩm.

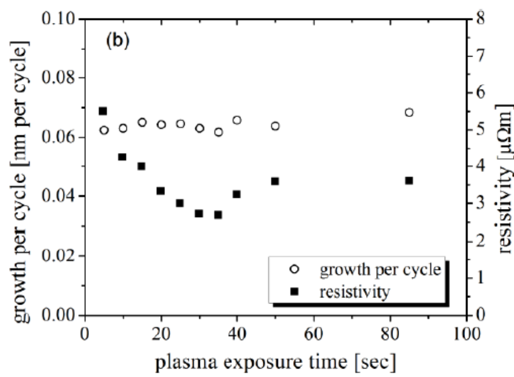

Figure 10: Effect of plasma exposure time on room temperature resistivity and growth per cycle from Ziegler, et al. Superconducting Science and Technology, 26, 2013 [63].

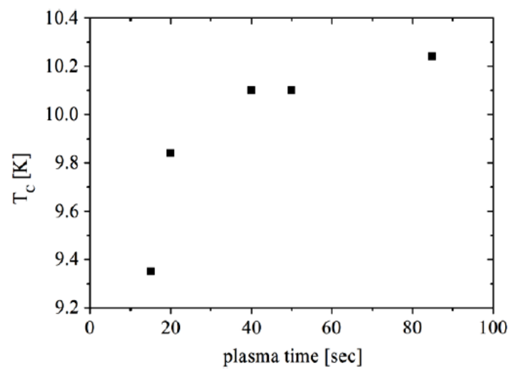

Figure 11: Influence of plasma exposure time on superconductive transition temperature from Ziegler, et al. Superconducting Science and Technology, 26, 2013 [63].

4 Experimental

4.1 ALD tool

Depositions were carried out in commercial Picosun SUNALE^{TM} R-200 Advanced ALD tool. Schematic representation of the reactor is shown in Figure 12. It is a hot wall, top flow type reactor capable of carrying out depositions from room temperature to 500 °C. It is equipped with Picoplasma^{TM} remote inductive plasma source system and Picoloader^{TM} Handyman single-wafer handling system consisting of load-lock and a robot. Typically load-lock was evacuated to ~$2 \cdot 10^{-5}$ hPa with turbo-molecular pump before transferring the sample into reaction chamber.

Reactor chamber is heated by elements located outside the reactor chamber in intermediate space between outer walls of the vacuum vessel and reactor chamber. Temperature of the reaction chamber and heater element is measured separately by thermocouples. Intermediate space has constant flow of nitrogen controlled by mass flow controller (MFC) keeping the intermediate space at higher pressure (typical pressure 2 hPa) than reactor chamber. No direct pressure of the reactor chamber is measured, but pressure of the intermediate chamber and exhaust line after powder trap is measured by a pressure transducer (PT). Typical pressure measurement value of the exhaust line is 0.2 hPa.

Precursors are fed through seven separate deposition lines of which six are injected in horizontal directions and one in vertical direction through the plasma unit as can be seen from Figure 12. The six horizontal precursor feed lines are equidistant from each other along circumference of a circle above the substrate. During deposition nitrogen gas (99.9999 %, Aga) flows through the six horizontal precursor feed lines while argon gas (99.9999 %, Aga) flow is maintained in the seventh line which comes through plasma unit. The nitrogen flow through the source feed lines is controlled by a MFC located before precursor sources and pressure in the line is also measured before the precursor source bottles by a PT. Through plasma unit it is possible to pulse nitrogen, hydrogen (99.9999 %, Aga), their mixture and ammonia with flow rate controlled manually by a needle valve. For thermal depositions a thermal lid is available and was used for most of the depositions blocking the flow through plasma unit and inserting a showerhead to promote uniformity of precursor flow.

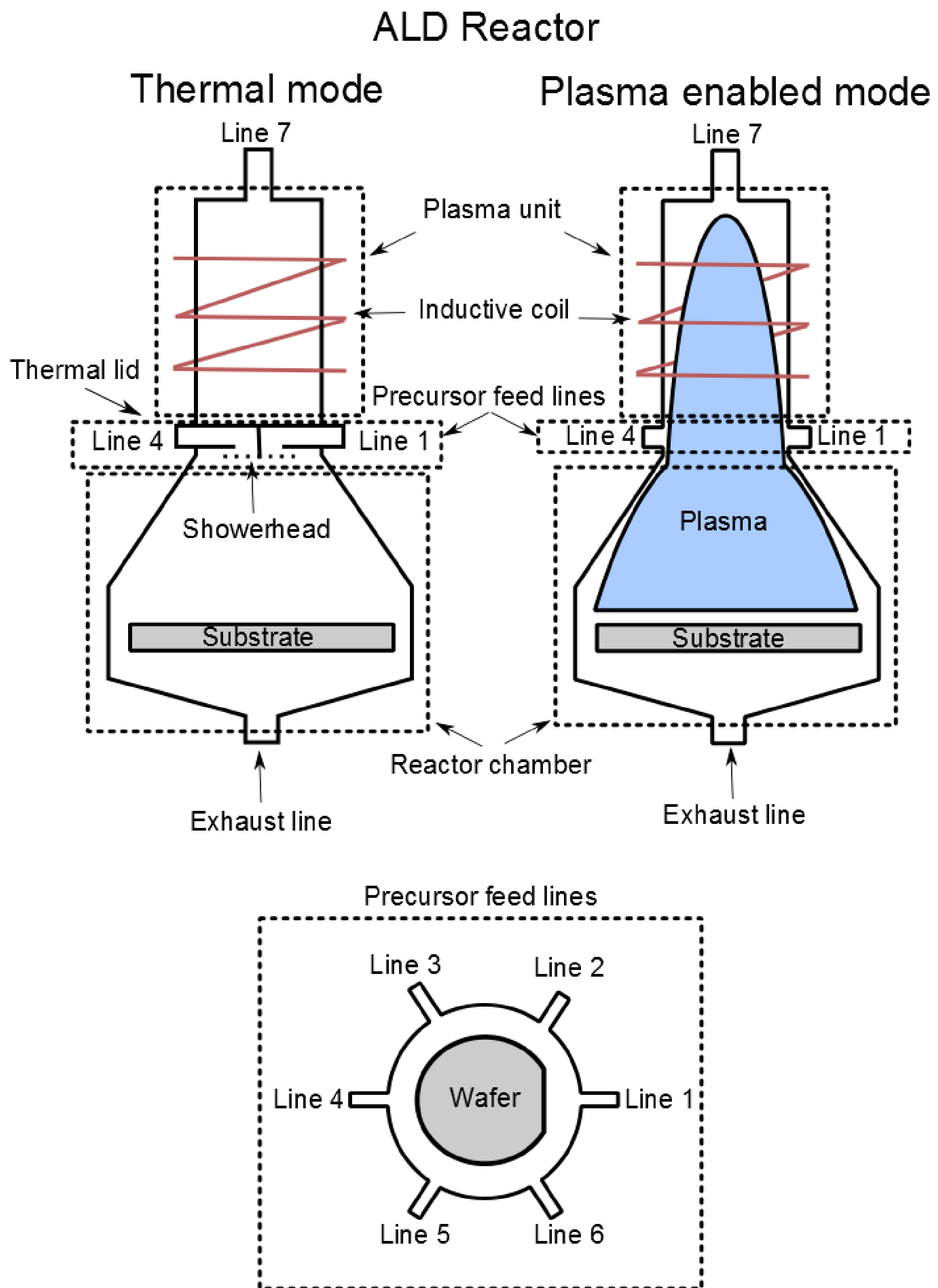

Figure 12: Schematic representation of Picosun SUNALE™ R-200 Advanced ALD tool in thermal mode and plasma enabled mode. In bottom image relative position of the precursor feed lines 1-6 is shown compared to location of primary flat of substrate wafer.

Source feed lines are located so that line 4 is located on the same side as load-lock. Wafer is always loaded in the load-lock so that primary flat of the wafer points away from the reactor chamber. Wafer rotates in the robot so that inside reactor chamber primary flat is on the opposite side of the line 4 as is shown in Figure 12. Directions of the wafer are matched by cardinal and ordinal directions. Direction of the primary flat is south and hence line 4 is on north side of the wafer. Rest of the source feed lines are located so that line 1 is in south, line 2 is in southeast, line 3 northeast, line 5 northwest and line 6 southwest. During deposition $NbCl_5$ (Research grade, SAFC Hitech) is pulsed through line 4 and NH_3 (99.999 %, AGA, additional purifying before tool) through line 6.

Picohot^{TM} 300 source system is used for $NbCl_5$ which has a bottom heater element around the source bottle, a top heater element, two manual closing valves and two pulsing valves. Between the two pulsing valves a capillary is placed to force majority of the carrier gas through the source bottle. One thermocouple is directly measuring source temperature and another is measuring heater element temperature to prevent overheating. Dose of a precursor in a pulse is dependent mainly on the temperature of the precursor bottle and corresponding vapor pressure of the precursor. There is no measurement tool to measure the dose and the line pressure in the source feed line does not change when pulsing valves are opened.

4.2 Deposition parameters

For all the depositions temperature of the valve block connecting the $NbCl_5$ source bottle to reactor chamber was kept at 150 °C and flow in the intermediate space was kept at 200 sccm (standard cubic centimeter per minute). Compilation of the deposition parameters and depositions done is shown in Appendix A.

Thermal depositions were carried out at reactor chamber temperatures between 400–500 °C and $NbCl_5$ source between 120–140 °C. $NbCl_5$ source line flow was varied from 150 to 275 sccm and NH_3 from 80 to 100 sccm. Other line flows are typically kept at 40 sccm. Pulse times used for $NbCl_5$ ranged from 0.5 to 2.5 s and purges from 3 to 10 s. For NH_3 pulse times used ranged from 0.1 to 1.5 s and purges from 3 to 15 s.

Thermal depositions using ABC cycle was done utilizing H_2 as additional reducing agent between $NbCl_5$ and NH_3 pulses and after NH_3 pulse. Depositions were carried out without thermal lid and H_2 gas was pulsed through plasma unit without plasma power. For these

depositions $NbCl_5$ was kept at 135 °C, line flow at 200 sccm, pulse time at 1.5 s and purge time at 5 s. For hydrogen 3 s pulse, 5 s purge, 53 sccm flow and 40 sccm argon flow was used and for ammonia 80 sccm flow, 1 s pulse and 6 s purge was used.

Plasma depositions were carried out at reactor chamber temperature of 500 °C, $NbCl_5$ source bottle temperature of 135 °C and $NbCl_5$ source line flow at 200 sccm. Pulse time used for $NbCl_5$ was 1.5 s and purge time 5 s. Three different plasmas were used: $Ar/H_2/N_2$, Ar/H_2 and Ar/NH_3. Argon flow was kept constant at 80 sccm except for Ar/NH_3 plasma where it was 40 sccm. N_2 flow was varied from 35 to 5.3 sccm and H_2 from 30 to 53 sccm. Plasma power was varied from 500 to 2000 W. For all the plasma depositions 1 s flow stabilization was used before plasma was ignited. Plasma power was on for 15 to 25 s and overall pulse time ranged from 16.5 to 27 s. Purge time used for NH_3 plasma was 10 s and for the rest 4 s was used.

Most of the depositions were carried out on thermally oxidized 100 mm <100> c-Si wafers, but some were 150 mm. The surface of these wafers was prepared with RCA-1 cleaning. In addition to this depositions were done also on 100 mm <100> c-Si which were cleaned with RCA-1 and dipped in HF and on top of ALD AlN deposited on RCA-1 cleaned 100 mm <100> c-Si.

AlN was deposited in the same reactor at 250 °C using $AlMe_3$ and NH_3 plasma. For $AlMe_3$ 0.1 s pulse length, 1.5 s purge length and 130 sccm line flow was used. NH_3 plasma parameters were 0.5 s flow stabilization, 2500 W plasma power on for 3.0 s, overall plasma pulse time 4.0 s, argon flow 50 sccm, NH_3 flow 35 sccm and purge length 1.0 s.

4.3 Characterization

NbN films were characterized by four point probe (FPP), wafer curvature, grazing incidence X-ray diffraction (GIXRD), X-ray reflectivity (XRR) and time of flight elastic recoil detection analysis (ToF-ERDA).

Cascade Microtech Inc. C4S-64/5S four point probe was used to measure resistance, R, of the films. Typically five points were measured at north, center, south, west and east points on the wafer individually and manually. Points measured were approximately 2 cm away from the edge. Measuring one wafer takes about 10 minutes. Resistivity, ρ, is calculated according to (13) by combining thickness, t, value obtained from XRR measurement.

$$\rho = 4.532 \cdot t \cdot R \tag{13}$$

Superconductivity of the samples was tested by dipping them into liquid helium and measuring resistance. This was performed by M.Sc. Mikko Kiviranta from VTT.

Wafer curvature measurements were used to measure stress of the grown films. The measurements were carried out by M.Sc. Hannele Heikkinen from VTT. Toho FLX 2320-S was used to measure the curvature of the wafer. It utilizes a laser beam to measure the surface radii of the wafer. By measuring the surface radii before and after the deposition, approximation of the stress in the film is possible to deduce from Stoney's formula (14)

$$\sigma_f = \frac{E_s t_s^2}{6t(1-\nu_s)}\left(\frac{1}{R} - \frac{1}{R_0}\right), \tag{14}$$

where E is Young's modulus, t is thickness, R and R_0 is measured curvature value and v is Poisson's ratio. Index s and f denote substrate and film respectively. Wafer curvature measurement gives more accurate values when thinner and larger wafers are used and deposition occurs only on one side. Single curvature measurement takes about 10 minutes.

GIXRD and XRR measurements were carried out using Philips X'pert Pro diffractometer using Cu Kα radiation. Some of the GIXRD and XRR measurements were carried out by M.Sc. Saima Ali and M.Sc. Sakari Sintonen. In GIXRD sample is fixed at an angle slightly above Brewster's angle to maximize signal from the film in contrast XRD. Detector rotates the specified range and collects diffraction data. X-rays are diffracted from atomic planes according to Bragg's law (15)

$$n\lambda = 2d\sin\theta \tag{15}$$

where λ is wavelength, d is distance between atomic planes and θ is angle between incident ray and scattering plane. Using GIXRD film material can be identified from diffraction peaks, but the peaks do not give data about texture of the film. In XRR x-rays are reflected from the surface. Reflectivity of the X-rays is sensitive to electron density and information about film thickness, interface roughness and mass density of the film is possible to obtain by fitting a theoretical curve to the measured curve. Fitting to the measured curve is performed manually using X'Pert Reflectivity software. Roughness values determined by XRR are not accurate and can be only used as approximate. Minimum sample size for GIXRD and XRR is 1x1 cm^2. For GIXRD minimum film thickness is about 20 nm. For XRR maximum film thickness is about 100 nm and minimum about 2 nm for

accurate thickness determination. Measurement and analysis of one simple sample takes about one hour for XRR and for GIXRD about three hours.

ToF-ERDA measurements were performed by M.Sc. Jaakko Julin and Ph.D. Timo Sajavaara at Jyväskylä University Accelerator Laboratory with home built measurement system consisting of Pelletron accelerator (1.7 MV terminal voltage), sputtering ion source and ToF-ERDA spectrometer. In ToF-ERDA measurements sample is bombarded with a beam of heavy ions which scatters atoms from the sample surface. In the measurements performed in this work a 13.6 MeV ^{63}Cu beam was used. Energy and velocity of the scattered atoms is measured allowing elemental identification. Depth profile is possible to determine qualitatively based on known scattering kinematics, scattering cross-sections and parameterized energy losses for incident ions and sample atoms. Optimal sample for ToF-ERDA measurements is a flat 1x1 cm^2 sample with film thickness of 50–100 nm. Measurement of one sample takes 1–4 hours and analysis 1–10 hours.

Taguchi method [64] was used to design some of the experiments. Orthogonal matrixes were created for chosen parameters and parameter levels. Table 4 shows Taguchi matrix for three parameters with two levels. After calculating signal-to-noise ratio for each parameter for chosen performance type effect of each parameter on this can be determined.

Table 4: Taguchi matrix for three variables with two levels.

Experiment number	Parameter 1	Parameter 2	Parameter 3
1	Level 1	Level 1	Level 1
2	Level 1	Level 2	Level 2
3	Level 2	Level 1	Level 2
4	Level 2	Level 2	Level 1

To minimize the performance of chosen parameter calculation of signal-to-noise ratio, SN, is done by equation (16)

$$SN = 10\log_{10}\left(\frac{S_m - V_e}{NV_e}\right) \quad (16)$$

where S_m is

$$S_m = \frac{(\sum T_i)^2}{N}, \tag{17}$$

V_e is

$$V_e = \frac{\sum T_i^2 - S_m}{N - 1} \tag{18}$$

T_i is value of individual measurement and N number of measurements. After calculating the SN ratio for each experiment, SN ratio of each parameter at each level is determined. This is done by calculating the average SN ratio of experiments with the parameter at that level. Finally the difference between the highest SN ratio and lowest SN ratio is determined and parameters are ranked from highest to lowest based on the SN ratio difference. The one with the largest difference affects the chosen performance type the most.

5 Results and discussion

5.1 Thermal depositions

5.1.1 Depositions with NH_3

First NbN depositions were attempted using Taguchi matrix method in order to find out the most relevant parameters regarding film growth. First matrix was formed based on three variables with two levels and is shown in Table 5. First deposition recipe was based on TiN recipe used in the same tool. Deposition temperature was 500 °C, $NbCl_5$ source bottle temperature 120 °C and purge time 10 s. For ammonia TiN parameters were used except for purge time, which was slightly longer, 12 s, were used (pulse time 0.1 s and flow 80 sccm). Flow in other deposition lines were kept at 40 sccm. 1000 cycles were deposited on thermally oxidized c-Si.

Table 5: Variables and values in first Taguchi matrix.

Deposition	$NbCl_5$ pulse length (s)	$NbCl_5$ line flow rate (sccm)	Double pulse
Sample 1	0.5	200	No
Sample 2	0.5	250	Yes
Sample 3	1.5	200	Yes
Sample 4	1.5	250	No

Erratic results were obtained and Taguchi matrix could not be calculated. In the first deposition by visual inspection film grew only in the middle in a circle of ~4 cm. In the second deposition no film was observed to grow at all. In the third deposition film grew asymmetrically, mostly on the edges and especially on spots where tweezers had touched the wafer. In the fourth deposition film was deposited uniformly only in the middle, in a circle of ~6 cm. XRR measurements were performed at the center of the samples, but only sample 4 was successfully measured. Sample 1 turned out to be too rough for XRR analysis, while for sample 2 and 3 XRR suggested that there was no film at all. Sample 4 turned out to have a film with density of 6.9 g/cm^3, roughness of 1.15 nm and thickness of 29 nm corresponding to growth rate of 0.29 Å/cycle. Growth rate is comparable to the growth

rate of 0.27 Å/cycle obtained by Alén et al. [58] for films grown at 500 °C. Resistivity of sample 4 was 657 μΩcm, which is slightly higher than the typical 500–600 μΩcm for thermal ALD NbN films without zinc.

Use of double pulse was attempted in order to increase the $NbCl_5$ supply to the substrate, but it appeared that $NbCl_5$ did not attach well enough on the surface and was removed during a purge step hence no growth or growth only in the edges. Regarding the increase in the area where film grew between sample 1 and 4, main cause was thought to be increase in $NbCl_5$ pulse length.

Next sample, #5, was deposited with 3330 cycles at 400 °C with $NbCl_5$ pulse length 1.5 s, purge length 5s, line flow 250 sccm. Source bottle temperature was increased from 120 to 125 °C to increase $NbCl_5$ vapor pressure. Ammonia pulse length was significantly increased from 0.1 to 1 s and purge length reduced to 6 s. The deposition resulted in metallic gray film deposited visibly uniformly on the whole 100 mm wafer. In order to decrease cycle times, purge times were further reduced to 3 s for both $NbCl_5$ and NH_3 in sample 6, which was deposited otherwise with the same parameters. The deposition resulted again in visibly uniform metallic gray film covering the whole wafer.

GIXRD and XRR measurements were performed on both samples. Both samples were found to be crystalline and (111) and (200) peaks were identified to correspond to cubic NbN phase. XRR measurements (Table 6) however showed that uniformity of the samples was poor and significant changes in the thickness were visible depending on the spot on the wafer. Difference in the growth rate between sample 5 and sample 6 was attributed to CVD type growth due to shortened purge times. Non-uniformity [(max-min)/(2·average)] of sample 5 based on XRR thickness measurements was 3 % and for sample 6, non-uniformity was 8 %. However, the measurement points especially on sample 5 do not represent the whole wafer.

Resistivity of the samples 5 and 6 was high compared to sample 4. Sample 5 had resistivity of about 1700 μΩcm and sample 6 about 1500 μΩcm. However, sample 4 was deposited at higher temperature and was denser.

Table 6: XRR results for sample 5 and 6. C, N, E, S and W corresponding to center, north, south, etc. represent point in the wafer where the measurement was performed.

Sample	Thickness (nm)	Density (g/cm^3)	Roughness (nm)
Sample 5_E	87.50	6.60	2.55
Sample 5_C	94.0	6.55	2.00
Sample 5_W	88.50	6.20	1.40
Sample 6_N	100.00	6.60	2.90
Sample 6_C	101.50	6.40	3.00
Sample 6_S	85.50	6.50	1.50
Sample 6_W	93.00	6.60	3.00
Sample 6_E	90.00	6.60	3.00

Based on the deposition recipe of sample 5 another Taguchi matrix (Table 7) was created to find parameters that had the biggest effect on resistivity. Reactor temperature, source bottle temperature and ammonia pulse length were chosen as variables. Reactor temperature was chosen as variable because of low resistivity of sample 4 compared to samples 5 and 6. $NbCl_5$ bottle temperature was chosen to be increased as it was suspected that supply of $NbCl_5$ was the limiting factor in film growth. Level of increase was chosen to be only 3 °C as vapor pressure increases exponentially with temperature. Ammonia pulse length was chosen because pulse time of 1 s seemed long compared to 0.1 s used or TiN deposition. 1500 cycles were deposited aiming for 50 nm film.

Table 7: Taguchi matrix for samples 7-10.

Deposition	Reactor temperature (°C)	$NbCl_5$ source bottle temperature (°C)	NH_3 pulse length (s)
Sample 7	400	125	1
Sample 8	400	128	0.5
Sample 9	475	125	0.5
Sample 10	475	128	1

Thickness, density and surface roughness of the samples was again measured by XRR and resistivity by FPP. Detailed results are shown in Appendix A. In Table 8 average value for thickness and resistivity is given.

Table 8: Thickness and resistivity of samples 7-10. Determined by XRR and FPP. Error is given as one sigma.

	Sample 7	Sample 8	Sample 9	Sample 10
Thickness (nm)	39.5±1.8	35.0±2.4	41.7±2.0	41.0±1.4
Resistivity (μΩcm)	1660±130	2070±250	900±60	920±20

To determine the effect of each parameter, signal-to-noise ratio of the variables was calculated according to (16). Results are shown in Table 9. Reactor temperature had largest value for max-min and hence it had the largest effect on resistivity. The larger SN ratio for a parameter at certain level means that at this level the performance was better. Based on this it was determined that in order to get lower resistivity it was better to use higher temperature, lower source bottle temperature and longer ammonia pulse. This knowledge was used to create recipe for sample 11.

Table 9: Calculated signal-to-noise ratio for each variable and level for Taguchi matrix for samples 7-10.

Level	Reactor temperature	$NbCl_5$ source bottle temperature	NH_3 pulse length
1	20.8	24.2	24.3
2	25.3	21.9	21.8
Max-Min	4.5	2.3	2.5

Sample 11 was deposited at 475 °C with bottle temperature of 125 °C and NH_3 pulse length of 1 s. Again 1500 cycles was deposited. Resistivity of sample 11 was calculated assuming thickness of 40 nm, which is based on thicknesses of samples 7–10. Detailed values of each single measurement are given in Appendix B. Average resistivity was 810±50 μΩm. It is better than for samples 7–10, which was expected as the recipe was based on best parameters determined from the Taguchi matrix.

Superconductivity of sample 11 was also tested by dipping it into liquid helium which cools it down to 4.2 K. However, resistivity increased with decreasing temperature as with semiconductors and no superconductive transition temperature was observed.

After the success with 150 mm wafers attempts were made on 200 mm wafers using the same recipe and further increasing the deposition temperature to 500 °C. First deposition on 200 mm wafer showed that film did not grow on the whole wafer. Wafer was lacking film near edge from area ranging from southwest to east. This pointed to the fact that center point of growth was not in the middle of the wafer.

Attempts were made to correct this by changing deposition flows. For samples 13 and 14 $NbCl_5$ line flow was adjusted to see the effect on film growth. Flow was increased to 275 sccm for sample 13, but the resulting film coverage shrank. Film was now growing approximately 2 cm from edge in southwest to east and 1 cm from northwest. For sample 14 $NbCl_5$ line flow was decreased to 150 sccm. This resulted in shift of the film center-point towards north and approximately 3 cm wide area from south edge was lacking film.

Ammonia flow was varied for sample 15. It was decided to test increasing ammonia flow from 80 scmm to 100 sccm while keeping the $NbCl_5$ line flow at 200 sccm. This, however, resulted in similar behavior as decreasing $NbCl_5$ line flow to 150 sccm. Film growth was again shifted towards north and 3 cm wide area in south was lacking film. Also the film did not appear to grow circularly compared to previous deposition.

Changing other line flows was tried for sample 17. It was decided to test changing the flows of lines one and two which located on the opposite side of $NbCl_5$ line. Flows were reduced to 20 sccm, but the resulting film grew asymmetrically, didn’t reach edges of the wafer anywhere and was visually non-uniform. Later it was realized that by setting the line flows in the tool below approximately 30 sccm it resulted in actual flow of the lines to stop completely.

$NbCl_5$ line flow was changed again for sample 18. It was concluded from samples 13 and 14 that decreasing the flow moved the center-point of growth in the wrong direction so that maybe the increase of the flow was too large. Hence the flow was now increased to 250 sccm in contrast to 275 sccm used for sample 13. Result was circular growth with slightly smaller coverage than with 200 sccm.

Next, the effect of temperature was tried for sample 19 by using the flow of 250 sccm for $NbCl_5$ line, but reducing temperature from 500 to 475 °C. Result was slightly smaller film coverage. Growing film on top of the whole 200 mm wafer was unsuccessful based on these tests and effort was directed to growing film on 150 mm wafers.

Using the best parameters observed so far ($NbCl_5$ source bottle 125 °C, line flow 200 sccm, pulse 1.5 s, purge 5 s, NH_3 line flow 80 sccm, pulse 1s, purge 6 s and flow in other lines at 40 sccm) films were deposited on 150 mm c-Si wafers that were cleaned with RCA1 and HF to undergo further analysis at collaborators. Five samples were deposited including temperature and thickness series. Temperature series consisted of deposition at 400, 450 and 500 °C. 3600 cycles were deposited aiming for 100 nm thickness. For thickness series samples were deposited at 500 °C. 1800 cycles and 900 cycles were deposited aiming for thicknesses of 50 nm and 25 nm.

The films were characterized by XRR, GIXRD, wafer curvature and ToF-ERDA. XRR results (Table 10) showed that thickness of deposited films increased with increasing deposition temperature and hence GPC increased. Also density increases from 6.65 g/cm^3 to 7.1 g/cm^3 with increasing temperature although it is still far from bulk density of cubic NbN, 8.47 g/cm^3 [23]. XRR measurement for MS2 was unsuccessful. This may be due to wafer being too bowed or surface too rough.

Table 10: Deposition conditions and results from XRR measurements for MS1-MS5. XRR measurement was unsuccesful for MS2.

	Deposition temperature (°C)	Cycles	Thickness (nm)	Growth per cycle (Å/cycle)	Density (g/cm^3)	Roughness (nm)
MS1	400	3600	105.5	0.29	6.65	3
MS2	450	3600	-	-	-	-
MS3	500	3600	125	0.35	7.1	3.5
MS4	500	1800	67	0.37	7.05	1.3
MS5	500	900	31.4	0.35	6.97	1.3

Growth rate is observed to increase from 0.29 to 0.36 Å/cycle with increasing temperature from 400 to 500 °C. Increase in growth rate with increasing temperature was observed also

by Alén et al. [58], which is contrary to what has been observed for thermal depositions for TiN and TaN where growth rate has remained more or less constant [40] [42] [55]. Uniformity of the NbN films was poor as with increasing deposition temperature south end of the wafer started having area of visible thinner film which became larger as temperature increased. Film grown at 400 °C was, however, visibly uniform.

Summary of ToF-ERDA results is shown in Table 11. Compositions are calculated by integrating depth profile within the film excluding interface and surface. In Figure 13 depth profile is shown for MS3 and in Appendix C for MS1-5. Oxygen peak is found at the surface corresponding to post-deposition oxidation. ToF-ERDA measurements showed that the films in general were very clean. Chlorine content decreased with increasing temperature as has been observed before [52] [46] [58]. Films were nitrogen rich with Nb/N ratio ranging from 0.8 to 0.9 which has been the case for all the thermal ALD NbN films deposited with NH_3. Alén et al. [58] observed ratio of 0.8 regardless of deposition temperature.

Table 11: Composition of samples MS1-5 measured by ToF-ERDA. Samples are very clean except for chlorine content which decreases with temperature.

	H (at%)	C (at%)	N (at%)	O (at%)	Cl (at%)	Nb (at%)
MS1	0.1±0.1	0.1±0.1	53±2	0.3±0.1	1.8±0.2	44±2
MS2	0.1±0.1	0.2±0.1	55±2	0.2±0.1	0.6±0.1	45±2
MS3	0.1±0.1	0.1±0.1	54±2	0.4±0.1	0.2±0.1	45±2
MS4	0.1±0.1	0.1±0.1	53±2	0.5±0.1	0.3±0.1	45±2
MS5	0.1±0.1	0.1±0.1	49±2	0.5±0.2	0.3±0.2	45±2

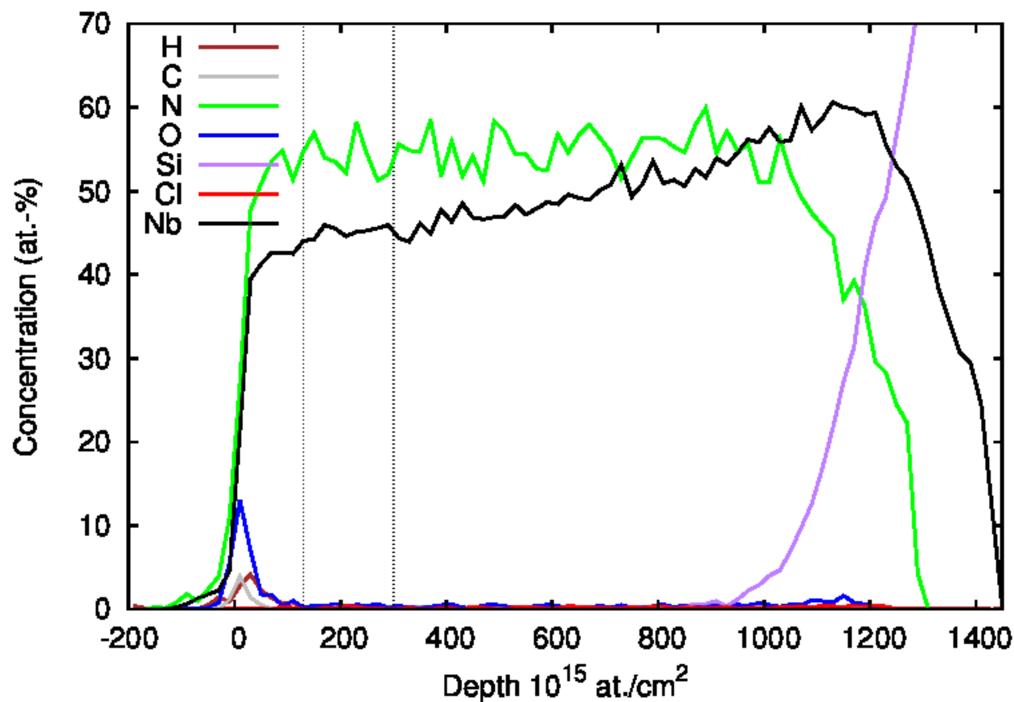

Figure 13: ToF-ERDA depth profile for MS3 showing low impurity concentration.

GIXRD revealed peaks again at similar positions as for sample 4 and showed that all the films were crystalline. Closer look at the diffraction peaks were done as Nb/N ratio determined from ToF-ERDA measurements resembled more Nb_4N_5 than stoichiometric NbN. In Figure 14 GIXRD results are presented with reference peak positions of cubic NbN and tetragonal Nb_4N_5. From this it is easy to see how easy it is to mix these two phases with each other. In Table 12 the observed 2θ angle is converted into d-value assuming cubic structure and compared to reference values for cubic NbN and tetragonal Nb_4N_5. It is visible that the values are closer to the reference values for Nb_4N_5. Ritala et al. [46] observed similar behavior for their films grown with NH_3. However, film grown with intermediate zinc pulses still had d-values closer to Nb_4N_5 than NbN even though the peaks shifted in the direction of cubic NbN. For both cubic NbN and tetragonal Nb_4N_5 all the strongest peaks for structures are visible in the measured 2θ range. However, as the lattice constant for Nb_4N_5 is larger, peaks at smaller angle, which was not measured in this measurement, might be visible.

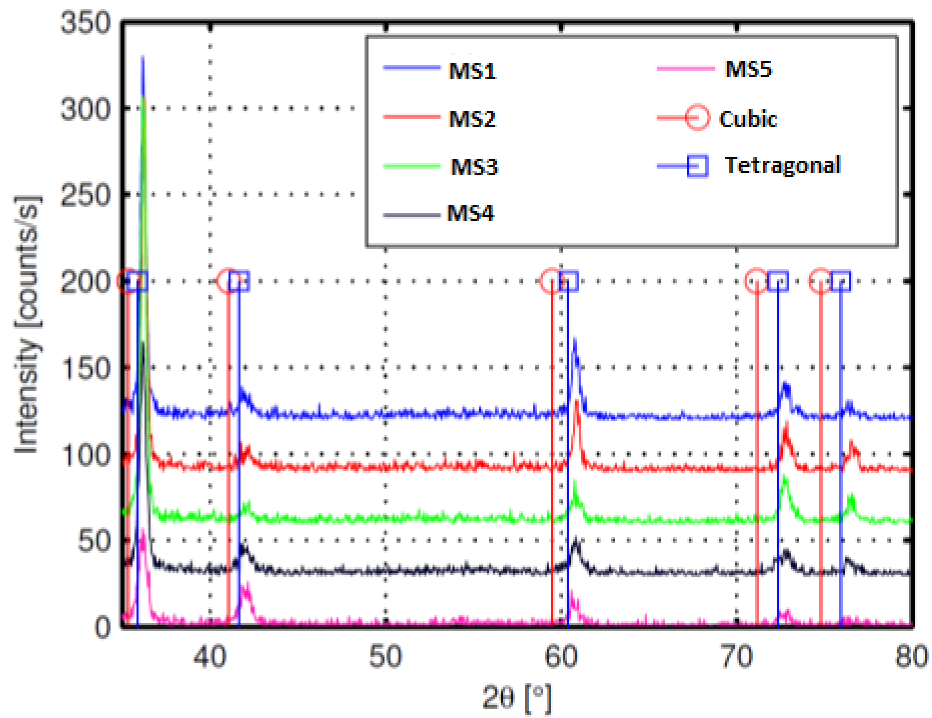

Figure 14: GIXRD results for MS1-5 samples and reference peak positions for cubic NbN and tetragonal Nb_4N_5. Peaks are shifted to larger angles than reference peaks for cubic NbN and are more close to tetragonal Nb_4N_5 reference peaks.

Table 12: Peak positions observed in GIXRD for MS1-5 and corresponding d-values for cubic structure are shown. For comparison reference values for cubic NbN [46] and tetragonal Nb_4N_5 [22] are given.

2θ (°)	d value (Å)	Cubic plane (hkl)	d value (Å)	Tetragonal plane (hkl)	d value (Å)
36.2	2.479	(111)	2.536	(211)	2.503
42.0	2.149	(200)	2.196	(310)(002)	2.166
60.8	1.522	(220)	1.553	(420)(312)	1.531
72.8	1.298	(311)	1.324	(421)(501)(213)	1.305
76.5	1.244	(222)	1.268	(422)	1.252

Another GIXRD measurement was performed to scan over this smaller range where peak for (101) plane is described to be medium strong in intensity which is same as the peak for (422) plane which is visible [22]. However, this peak was not detected in the measurement,

which might be due to increased background noise at lower angles. Due to this even with the ToF-ERDA results and GIXRD data it is not possible say for certain whether the phase is cubic or tetragonal although it would seem more likely that the film is tetragonal.

Residual stress of the films was determined from wafer curvature measurements using thickness values measured by XRR. Residual stress was found to increase from 1500 to 1700 MPa with temperature increasing from 400 to 500 °C as was expected due to thermal mismatch between substrate and the film being significant factor in formation of residual stress. However, drop in the residual stress from 1700 MPa for film with 3600 and 900 cycles to 1500 MPa for film deposited for 1800 cycles was unexpected and reason for this unclear. The drop is not within estimated measurement error which was below 100 MPa.

Deposition of sample 23 was carried out on thermally oxidized silicon using same deposition parameters as MS3–5. Amount of cycles deposited was 900. Thickness of the film was measured by XRR to be 51.5 nm corresponding to growth rate of 0.57 Å/cycle. The increase of growth rate between two films grown with same parameters is significant. MS3–5 had average growth rate of 0.36 Å/cycle. This might be due to non-uniformity of the film and measurement might have not been done from same point on the wafer. Non-uniformity determined from sheet resistance measured by FPP from five points (north, center, south, east and west) was 37%. This uniformity value is not directly comparable to values obtained earlier for samples 5 and 6, which was determined from XRR measurements. Observed growth rate is also higher than what is observed in literature for NbN or TaN, however for TiN similarly high growth rates has been observed [44].

Supply of $NbCl_5$ was thought to be factor limiting the film growth. Sample 25 was deposited with increased $NbCl_5$ source bottle temperature to 135 °C. Resulting was characterized by XRR and FPP. XRR results determined thickness of 55.2 nm, which corresponds to growth rate of 0.61 Å/cycle. Film was visually uniform pointing to the fact that supply of $NbCl_5$ was indeed limiting factor. Non-uniformity of the film, however, was still an issue. Non-uniformity decreased from sample 23, but was still 20%. It was suspected that the purge times might not be long enough and CVD type growth was contributing to film growth.

Increased purge times were used when samples 27-29 were deposited. NH_3 purge time was increased up to 15 s and $NbCl_5$ purge time up to 10 s. Pulse lengths used were 1.5 s for

$NbCl_5$ and 1 s for NH_3. Table 13 summarizes results from the depositions. Thickness was found to decrease from increasing NH_3 purge to 10 s which points to the existence of CVD type growth with lower purge time. Further decreasing the purge times did not have significant effect. Uniformity of the grown films was still poor around 20 %.

Table 13: Results from extending purge times for NH_3 and $NbCl_5$ in terms of thickness, resistivity and non-uniformity.

	$NbCl_5$ purge (s)	NH_3 purge (s)	Thickness (nm)	Resistivity (µΩcm)	Non-uniformity (%)
Sample 25	5	6	55.2	750	20
Sample 27	5	10	41.3	710	18
Sample 28	5	15	41.5	700	14
Sample 29	10	15	40	630	21

In next depositions pulse times for $NbCl_5$ and NH_3 was altered to determine whether that would solve the problem with uniformity and verify that we reach saturation with pulse lengths. Purge times used for the deposition were chosen to be 5 s for $NbCl_5$ and 10 s for NH_3. Table 14 summarizes varied deposition parameters and results. Growth rate increases (0.41 to 0.50 Å/cycle) with increasing $NbCl_5$ pulse length over the whole range from 0.5 to 2.5 s. After 1.5 s, however, uniformity is not improved.

Due to increase of thickness over the whole range, sample 33 with increased source bottle temperature was deposited to increase $NbCl_5$ dose in the pulse. It was found to decrease the non-uniformity from 18 to 12 % and increase thickness slightly from 44.8 to 46.4 nm, but small decrease in resistivity from 700 to 740 µΩcm was observed as well.

Best uniformity is observed for film with 0.5 s NH_3 pulse, but with increasing pulse length growth rate is observed to increase clearly from 0.43 to 0.51 Å/cycle showing that growth is not saturated yet. Growth rate appears to saturate after 1 s pulse to approximately 0.50 Å/cycle. By increasing the NH_3 pulse to 1.5 s uniformity and resistivity is improved slightly compared to 1 s pulse.

Table 14: Results from variation of $NbCl_5$ and NH_3 pulse lengths and increase of $NbCl_5$ source bottle temperature in thickness, resistivity and non-uniformity.

	$NbCl_5$ source bottle (°C)	$NbCl_5$ pulse (s)	NH_3 pulse (s)	Thickness (nm)	Resistivity (μΩcm)	Non-uniformity (%)
Sample 31	135	0.5	1	36.7	780	61
Sample 27	135	1.5	1	41.3	710	18
Sample 32	135	2.5	1	44.8	700	18
Sample 35	135	2.5	0.5	39.5	700	8
Sample 34	135	2.5	1.5	45.8	670	14
Sample 33	140	2.5	1	46.4	740	12

5.1.2 Depositions with H_2 and NH_3

Use of hydrogen as additional reducing agent was tried to produce cubic NbN. Idea was to emulate zinc, but without the contamination issues. Hydrogen was pulsed through the plasma unit without plasma activation at 500 °C. First deposition consisted of using hydrogen as intermediate pulse between $NbCl_5$ and NH_3. For $NbCl_5$ and NH_3 same parameters were used as in sample 25: $NbCl_5$ source bottle temperature 135 °C, pulse length 1.5 s, purge length 5 s, line flow 200 sccm, and NH_3 pulse length 1 s, purge length 6 s and flow 80 sccm. Hydrogen pulse length was 3 s, purge length 5 s and line flow 53 sccm.

Result of the deposition was similar to Sample 2 and 3 where double pulse was used for $NbCl_5$. Film was not deposited uniformly on topside and most of the deposition occurred on the backside of the wafer. Again it appeared that adsorbed $NbCl_5$ was blown off during hydrogen pulse as was suspected to be the case with the secondary $NbCl_5$ pulse for samples 2 and 3. Thickness of the grown film was 29.8 nm corresponding to growth rate of 0.33 Å/cycle, which is almost half of the growth rate for sample 25.

This would point to the fact that hydrogen does not react with the adsorbed $NbCl_5$. This is also supported by literature where thermodynamic study was done on reducing ability of zinc and hydrogen on $NbCl_5$. It was determined that hydrogen requires higher temperatures (above 750 °C) than zinc (approximately 500 °C) to reduce $NbCl_5$ [65]. This is also supported

by the thermodynamic study done by Ritala et al. [33] (Figure 6) where it was determined that reaction with ammonia and hydrogen is thermodynamically less favorable than reaction with just ammonia.

5.1.3 Summary of thermal depositions

Temperature is observed to affect growth rate. It increases with increasing temperature and growth rate at 500 °C is approximately 0.50 Å/cycle which is higher than what is observed for NbN and TaN in literature. However, for TiN, which typical growth rate is similar to NbN and TaN, growth rate as high as 0.6 Å/cycle has been observed [44].

Resistivity of the deposited films, approximately 700 µΩcm, is similar to literature (best ones 550-600 µΩcm [58] [46] [52]) values for films grown with NH_3. No superconductivity is observed in our films and GIXRD and ToF-ERDA results suggest that films are tetragonal Nb_4N_5 instead of cubic NbN.

Use of hydrogen as additional reducing agent requires higher temperatures and does not result in cubic NbN.

5.2 Plasma depositions

5.2.1 Depositions with $Ar/H_2/N_2$ plasma

Plasma depositions were done to introduce more reactive precursor that would be able to reduce $NbCl_5$ from oxidation state +V to +III as thermal depositions pointed to the fact that reducing capability of NH_3 was insufficient.

First plasma deposition (sample 26) was attempted at 500 °C using recipe which was based on plasma TiN recipe used with same kind of ALD tool. $NbCl_5$ was pulsed using similar parameters as was used for thermal depositions: source bottle temperature 135 °C, line flow 200 sccm, pulse length 1.5 s and purge time 5 s. Argon flow was kept constant at 80 sccm, while during plasma pulse, flow rate of nitrogen was 35 sccm and hydrogen 30 sccm. Flow was stabilized for 1 s before initiation of 1000 W plasma power. Plasma power was on for 25 s after which hydrogen and nitrogen flow was left on for additional 1 s adding up to total plasma pulse time of 27 s. After plasma pulse 4 s purge step was done.

Resulting film was visibly uniform. Non-uniformity of the film (9 %) based on sheet resistance was better than for thermal processes. The thickness measured by XRR was

71.5 nm corresponding to growth rate of 0.79 Å/cycle. This is higher than for thermal processes, but it is typical that plasma processes have higher growth rate than thermal processes. Density (7.2 g/cm^3) was slightly higher than measured for thermal processes (highest 7.1 g/cm^3). Resistivity of the film was 770 µΩcm, which is slightly higher than the values observed for thermal processes.

Changes to nitrogen and hydrogen flow rate were done in the recipe for sample 39. Nitrogen flow rate was decreased from 35 to 5.3 sccm while hydrogen flow rate was increased from 30 to 53 sccm to get 0.1 nitrogen-hydrogen partial flow ratio. Kim et al. [56] had grown cubic TaN films using N_2/H_2 partial pressure ratio between 0.025–0.035.

The film had resistivity of 490 µΩcm, which is lowest that we obtained for any film. Thickness of the film was 20.7 nm determined by XRR. Growth rate was 0.52 Å/cycle, which was significantly lower than what was observed for sample 26 (0.79 Å/cycle). Density was also lower than for sample 26, only 6.8 g/cm^3. This is unexpected as lower density is often accompanied with higher growth rate due to impurities. Also lower density has usually correlated with higher resistivity. The sample was also tested for superconductivity, but no superconductive transition temperature was found down to 4.2 K.

Increased plasma power was used for next sample. Sample 41 was deposited with increased plasma power to 1500 W. Resulting film had thickness of 22.1 nm corresponding to growth rate of 0.55 Å/cycle. Resistivity was higher than for sample 39, 1560 µΩcm. This might be due to increased nitrogen content in the film from more reactive nitrogen. However, this is only speculation and has not been validated in any way. GIXRD revealed again peaks at similar positions as MS1–5.

Shorter plasma exposure time was used for samples 43 and 44. Plasma exposure time decreased to 15 s from previous 25 s. Sample 43 was deposited using 1000 W plasma power. Resulting film was less uniform than previously (non-uniformity 24 %) and sheet resistance was tenfold compared to sample 39 (2900 Ω/□) pointing to the fact that plasma power was on for too short time period. Sample 44 was deposited using 500 W plasma power. Uniformity of the film was further decreased and sheet resistance grew over tenfold.

Enhanced crystallinity of NbTiN films has been reported on top of amorphous AlN layer [59]. Also AlN layer is dielectric making it possible to realize all nitride conductor-insulator

structures. Hence ~25 nm AlN was used as a seed layer for sample 48. AlN nitride was deposited in-situ prior to NbN deposition. NbN was deposited using same parameters as was used for sample 39.

Resulting film was visually uniform. AlN substrate had clear effect on the growth of NbN as growth rate was only 0.35 Å/cycle. Thickness was 31.9 nm and density 6.8 g/cm^3. Resistivity was 1560 µΩcm, which was high compared to sample 39. However, non-uniformity was only 3 % making it the most uniform film grown. This was result of only changing substrate from thermal SiO_2 to in-situ grown AlN. Uniformity of the samples deposited on silicon was not determined at any point so comparison to those cannot be made. GIXRD revealed peaks again at similar positions as MS1–5.

5.2.2 Depositions with Ar/H_2 plasma

Depositions using hydrogen plasma were used to confirm whether it is possible to reduce $NbCl_5$ to metallic niobium. In literature deposition of metallic tantalum and titanium has been realized using hydrogen plasma [66] [67]. Deposition of metallic niobium would also prove that reduction of $NbCl_5$ using hydrogen plasma is possible, which is required for deposition of cubic NbN. Reported tantalum and titanium films proved to be extremely sensitive to oxidation [66], which is why on top of the first film thin ~2 nm alumina barrier film was deposited.

First deposition (sample 30) was performed using the same parameters as was used for sample 26 with Ar/N_2/H_2-plasma with the exception of nitrogen valve being closed.

The resulting film appeared visibly uniform with metallic gray color. Thickness of the film was measured by XRR and was determined to be 76.5 nm, which corresponds to growth rate of 0.85 Å/cycle. This was similar as was observed for sample 26. Density was 7 g/cm^3, which is slightly less than in sample 26. Resistivity, however, had improved to 530 µΩcm. Non-uniformity was roughly the same as for sample 26, 11 %.

GIXRD was performed to determine the structure of deposited material. Peaks for niobium were not found, but the peaks corresponded to the peaks found for samples MS1-5. Figure 15 shows GIXRD results of sample 30 compared to MS3. According to GIXRD the deposited film was NbN instead of metallic niobium.

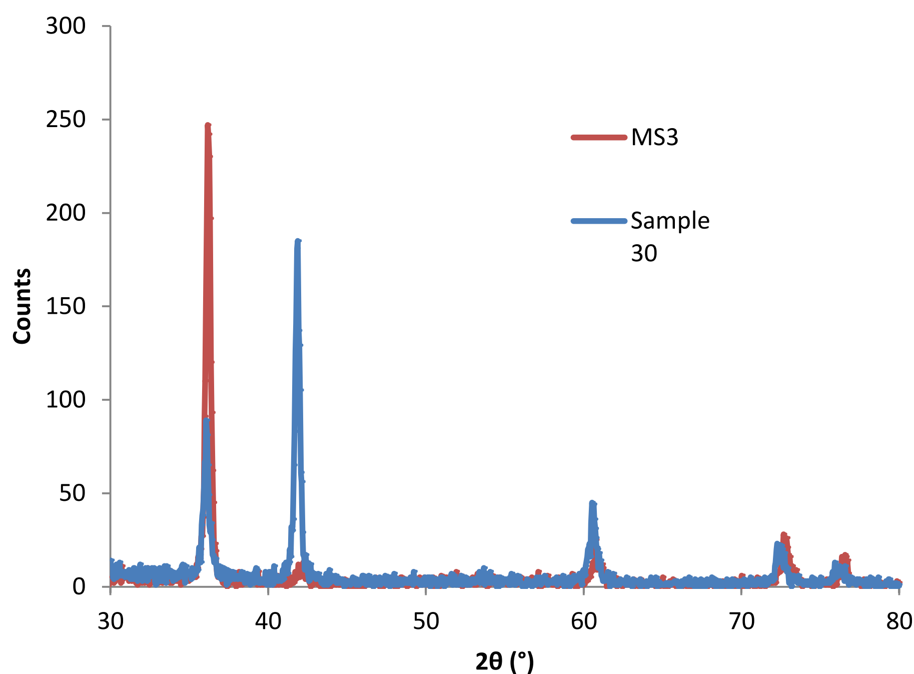

Figure 15: GIXRD results for sample 30 compared to GIXRD results for MS3 showing peaks at similar positions.

Sample 30 was tested for superconductivity due to encouragingly low resistivity, but no superconductive transition temperature was found down to temperature of liquid helium, 4.2 K.

Attempt was made to deposit film with increased plasma power to 2000 W. The result was resistive yellow film with resistivity over 80000 µΩcm. The thickness of the film was only 5.15 nm and growth rate 0.13 Å/cycle.

Only source for nitrogen in the reactor was inert nitrogen which flow through lines 1-6 constantly even during plasma pulse. This nitrogen is incorporated into the film. To validate this, sample 49 was deposited on c-Si for ToF-ERDA analysis using otherwise same parameters except hydrogen flow was increased to 53 sccm.

ToF-ERDA results showed that in the film 26 at% nitrogen was incorporated and 39 at% of niobium, but also that 30 at% of oxygen was incorporated. The source of oxygen was determined to be from chamber as deposition prior to this had utilized oxygen plasma. Metallic titanium and tantalum depositions have been found to be extremely sensitive to any oxygen or water present as mentioned previously. However, the results show that nitrogen is incorporated into the film from the flow of nitrogen through lines 1-6 and it is

speculated that without the incorporation of oxygen, nitrogen content would be higher. Incorporation of hydrogen into the film was not observed; hydrogen content in the film was less than 0.2 at%. Incorporation of hydrogen has been observed in PEALD TiN films deposited with N_2/H_2-plasma although the depositions are carried out at lower temperatures [47] [50]. ToF-ERDA measurement also revealed 5 at% incorporation of metals in mass-range of 50–60 g/mol (from vanadium to nickel). These are all possible alloying elements of steel and none of the metals have been deposited in the reactor, so it is suspected that plasma has detached some steel from chamber or plasma unit.

5.2.3 Depositions with NH_3 plasma

NH_3-plasma was used to deposit sample 42. For $NbCl_5$ same parameters was used as was used in all previous plasma deposition: $NbCl_5$ source bottle temperature 135 °C, line flow 200 sccm, pulse length 1.5 s and purge length 5 s. NH_3 plasma parameters used were 1 s flow stabilization before igniting 1000 W plasma power on for 15 s with 0.5 s post pulse stabilization and 10 s purge.

Resulting film was determined to be 47.7 nm thick by XRR. Growth rate was 0.53 Å/cycle. Non-uniformity was 10 %, which was similar to what was obtained for PEALD films. Resistivity, however, was higher 2810 µΩcm. The reason was initially thought to be excess amount of nitrogen in the film, but as with sample 49 oxygen plasma had been used prior to the deposition and film could have had large amount of oxygen incorporated also. However, no measurements were performed to validate this. GIXRD showed again peaks at similar positions as with MS3 and sample 30.

5.2.4 Summary of plasma depositions

Plasma depositions were carried out using $Ar/H_2/N_2$-, Ar/H_2- and Ar/NH_3-plasma. Growth per cycle was observed to be higher than for thermal processes, typically 0.5–0.8 Å/cycle. Best resistivity, 490 µΩcm, was obtained for a film deposited with $Ar/H_2/N_2$-plasma which was lower than what was observed for thermal films deposited. However, no superconductive transition temperature was found down to 4.2 K. GIXRD revealed peaks corresponding to those obtained for thermal processes.

Deposition using Ar/H_2-plasma revealed incorporation of nitrogen into the films from reactor atmosphere. This prevented adjusting nitrogen content in the films in order to obtain cubic NbN.

6 Conclusion and outlook

Thermal processes using NH_3 are unable to reduce $NbCl_5$ from +V oxidation state to +III. More reactive precursor is required. Use of hydrogen as intermediate pulse does not work as higher temperatures are required for hydrogen to be active.

The inability to deposit superconductive NbN films with thermal process without using zinc reduces the advantages of ALD NbN films. However, plasma processes should be able to produce higher quality films, which is important when superconductivity concerned. Plasma processes developed in this work are first published results for PEALD with $NbCl_5$.

Plasma processes should be able to reduce $NbCl_5$ as has been the case with $TaCl_5$, but controlling the nitrogen content in the film was not possible because the chamber atmosphere was not inert. Operation under argon atmosphere is required. This requires hardware changes to be made to the ALD tool.

In order to obtain high-quality films reaction chamber conditions should be controlled better. This includes removal of oxygen and water from the chamber prior to deposition and passivation of chamber walls with known film to reduce possible contamination.

ALD films usually have good non-uniformity around 1 %. However, uniformity of the films deposited in this work remained a problem although not much effort was put to solve this. Films deposited on top of SiO_2 behaved similarly between each other: film was thicker in northwest and thinner in southeast. By adjusting deposition line flows this might be fixed. However, the significantly improved uniformity on top of AlN complicates the analysis of the reason for low uniformity. Whether the problem is with the substrates, with the deposition parameters or both? Determination of the uniformity was also inaccurate as measurement was done manually over 5 points. Use of sheet resistance mapping tool would give more reliable and reproducible results.

Use of sheet resistance mapping tool would also be advantageous when determining the saturation with pulse lengths and purge lengths, which were not determined with enough precision due to limited access to XRR. Sheet resistance map coupled with multiple XRR measurements over the sample would give better insight into saturation of growth in different parts of the sample.

Taguchi method is not suitable in the early stages of ALD process development because some runs may not produce meaningful results at all. However, it might be suitable at later stages especially if determining the chosen performance characteristic is straightforward. In this study chosen performance characteristic was chosen to be sheet resistance, which inversely correlates to thickness. This was unsuccessful choice as many other characteristics of the film also affect sheet resistance, which dependent on other deposition parameters. Analysis of the Taguchi matrix led to conclusions detrimental to uniformity.

Deposition of superconductive films by ALD would allow further miniaturization of superconductive electronics as has been the case with microelectronics. Deposition of high quality, homogenous and pin-hole free films is essential for modern detector applications like superconductive single-photon detector (SSPD) and kinetic inductance detector (KID). In superconductive nanowire single photon detectors (SNSPD) film thicknesses are typically below 5 nm as smaller cross-sectional area increases sensitivity and detection efficiency of the detector. Similarly for KIDs small cross-sectional areas are preferred in order to reduce noise and increase responsivity. This size range is well suitable for ALD films and benefits from its precise thickness control whereas it is close to the minimum thickness for sputtering. Conformal deposition by ALD might also open up new types of applications that have not been possible to realize by sputtering.

Optimizing deposition process for superconductive microelectromechanical system (MEMS) applications is more complicated than typical optimization for either superconductive applications or MEMS applications. This is because of simultaneous optimization of superconductive properties with mechanical properties without losing performance in the other.

References

[1] W.-M. Li, "Recent developments of atomic layer deposition processes for metallization," *Chemical Vapor Deposition,* vol. 19, pp. 82-103, 2013.

[2] Beneq Oy, "nSILVER® Anti-tarnish Coating," [Online]. Available: http://www.beneq.com/nsilver-anti-tarnish-coating.html. [Accessed 06 11 2014].

[3] L. E. Toth, Transition metal carbides and nitrides, Academic Press, 1971.

[4] D. Heinrich, Influence of material and geometry on the performance of superconducting nanowire single-photon detectors, Doctoral Dissertation, Karlsruhe: KIT Scientific Publishing, 2013.

[5] M. Rösch, Development of lumped element kinetic inductance detectors for mm-wave astronomy at the IRAM 30 m telescope, Doctoral Dissertation, Karlsruhe: KIT Scientific Publishing, 2013.

[6] J.-O. Carlsson and P. M. Martin, "7. Chemical Vapor Deposition," in *Handbook of Deposition Technologies for Films and Coatings - Science, Applications and Technology*, 3rd ed., P. Martin, Ed., William Andrew Publishing, 2010.

[7] R. W. Johnson, A. Hultqvist and S. F. Bent, "A brief review of atomic layer deposition: from fundamentals to applications," *Materials Today,* vol. 17:5, pp. 236-246, 2014.

[8] M. V., M. Leskelä, M. Ritala and P. R. L., "Crystallinity of inorganic films grown by atomic layer deposition: Overview and general trends," *Journal of Applied Physics,* vol. 113:2, p. 021301, 2013.

[9] R. L. Puurunen, "A Short History of Atomic Layer Deposition: Tuomo Suntola's Atomic Layer Epitaxy," *Chemical Vapor Deposition,* vol. 20 , 2014 (in press).

[10] G. N. Parsons, J. W. Elam, S. M. George, S. Haukka, H. Jeon, W. M. M. Kessels, M. Leskelä, P. Poodt, M. Ritala and S. M. Rossnagel, "History of atomic layer deposition

and its relationship with the American Vacuum Society," *Journal of Vacuum Science & Technology A,* vol. 31, p. 050818, 2013.

[11] M. Ritala and J. Niinistö, "4. Atomic Layer Deposition," in *Chemical Vapour Deposition - Precursors, Processes and Applications*, A. C. Jones and M. L. Hitchman, Eds., Royal Society of Chemistry, 2009, p. 175.

[12] L. Hiltunen, M. Leskelä, M. Mäkelä, L. Niinistö, E. Nykänen and P. Soininen, "Nitrides of titanium , niobium, tantalum and molybdenum grown as thin films by the atomic layer epitaxy method," *Thin Solid Films,* vol. 166, pp. 149-154, 1988.

[13] R. L. Puurunen, "Surface chemistry of atomic layer deposition: A case study for the trimethylaluminum/water process," *Journal of Applied Physics,* vol. 97, p. 121301, 2005.

[14] T. Suntola, "Atomic layer epitaxy," *Materials Science Reports,* vol. 4, no. 7, pp. 261-312, 1989.

[15] S. M. George, "Atomic layer deposition: An overview," *Chemical Reviews,* vol. 110, pp. 111-131, 2010.

[16] H. B. Profijt, S. E. Potts, M. C. M. van de Sanden and W. M. M. Kessels, "Plasma-assisted atomic layer deposition: basics, opportunities, and challenges," *Journal of Vacuum Science & Technology A,* vol. 29, p. 050801, 2011.

[17] S. B. S. Heil, J. van Hemmen, C. J. Hodson, N. Singh, J. H. Klootwijk, F. Roozeboom, M. C. M. van de Sanden and W. M. M. Kessels, "Deposition of TiN and HfO2 in a commercial 200 mm remote plasma atomic layer deposition reactor," *Journal of Vacuum Science & Technology A,* vol. 25, no. 5, p. 1357, 2007.

[18] S. Anders, M. Blamire, F.-I. Buchholz, D.-G. Crété, R. Cristiano, R. Febvre, L. Fritzsch, A. Herr, E. Il'ichev, J. Kohlmann, J. Kunert, H.-G. Meyer, J. Niemeyer, T. Ortlepp, H. Rogalla, T. Schurig, M. Siegel, R. Stolz, E. Tarte, H. J. M. ter Brake, H. Toepfer, J.-C. Villegier, A. M. Zagoskin and A. B. Zorin, "European roadmap on superconductive electronics - status and perspectives," *Physica C,* vol. 470, pp. 2079-2126, 2010.

[19] L. Koutsokeras, Growth, structure and electronic properties of ternary transition metal nitrides thin films, Doctoral thesis, Universite de Poitiers, 2010, p. 17.

[20] E. Langereis, S. B. S. Heil, M. C. M. van de Sanden and W. M. M. Kessels, "In situ spectroscopic ellipsometry study on the growth of ultrathin TiN films by plasma-assisted atomic layer deposition," *Journal of Applied Physics,* vol. 100, p. 023534, 2006.

[21] L. Fred, "Developing a theoretical relationship between electrical resistivity, temperature, and film thickness for conductors," *Nanoscale Research Letters ,* vol. 6, no. 1, p. 636, 2011.

[22] N. Terao, "New phases of niobium nitride," *Journal of the Less-Common Metals,* vol. 23, pp. 159-169, 1971.

[23] D. R. Lide, Ed., CRC Handbook of chemistry and physics, 89th ed., Boca Raton: CRC, 2008.

[24] A. Shoji, S. Kiryu and S. Kohjiro, "Superconducting properties and normalstate resistivity of singlecrystal NbN films prepared by a reactive rfmagnetron sputtering method," *Applied Physics Letters,* vol. 60, no. 13, p. 1624, 1992.

[25] Z. Wang, A. Kawakami, Y. Uzawa and B. Komiyama, "Superconducting properties and crystal structures of singlecrystal niobium nitride thin films deposited at ambient substrate temperature," *Journal of Applied Physics,* vol. 79, no. 10, p. 7837, 1996.

[26] M. F., I. A. S., S. Olafsson and J. T. Gudmundsson, "Growth and in-situ electrical characterization of ultrathin epitaxial TiN films on MgO," *Thin Solid Films,* vol. 519, pp. 5861-5867, 2011.

[27] T. Shiino, S. Shiba, N. Sakai, T. Yamakura, L. Jiang, Y. Uzawa, H. Maezawa and S. Yamamoto, "Improvement of the critical temperature of superconducting NbTiN and NbN thin films using the AlN buffer layer," *Superconductor Science and Technology,* vol. 23, p. 045004, 2010.

[28] N. Arshi, J. Lu, Y. K. Joo, C. G. Lee, J. H. Yoon and F. Ahmed, "Influence of nitrogen gas flow rate on the structural, morphological and electrical properties of sputtered TiN

films," *Journal of Materials Science: Materials in Electronics,* vol. 24, pp. 1194-1202, 2013.

[29] M. Kawamura, Y. Abe, H. Yanagisawa and K. Sasaki, "Characterization of TiN films prepared by a conventional magnetron sputtering system: influence of nitrogen flow percentage and electrical properties," *Thin Solid Films,* vol. 287, pp. 115-119, 1996.

[30] P. Patsalas and S. Logothetidis, "Optical, electronic, and transport properties of nanocrystalline titanium nitride thin films," *Journal of Applied Physics,* vol. 90, no. 9, p. 4725, 2001.

[31] R. Fix, R. G. Gordon and D. M. Hoffman, "Chemical vapor deposition of titanium, zirconium, and hafnium nitride thin films," *Chemistry of Materials,* vol. 3, pp. 1138-1148, 1991.

[32] C. H. Winter, "The chemical vapor deposition of metal nitride films using modern metalorganic precursors," *Aldrichimica Acta,* vol. 33, no. 1, pp. 3-12, 2000.

[33] M. Ritala, M. Leskelä, E. Rauhala and P. Haussalo, "Atomic layer epitaxy growth of TiN thin films," *Journal of Electrochemical Society,* vol. 142, no. 8, pp. 2731-2737, 1995.

[34] G. Oya and Y. Onodera, "Transition temperatures and crystal structures of singlecrystal and polycrystalline NbNx films," *Journal of Applied Physics,* vol. 45, no. 3, p. 1389, 1974.

[35] R. A. Fischer and H. Parala, "9. Metal-organic chemical vapour deposition of refractory transition metal nitrides," in *Chemical Vapour Deposition - Precursors, Processes and Applications*, A. C. Jones and M. L. Hitchman, Eds., Royal Society of Chemistry, 2009.

[36] X. Chen, H. L. Frisch, A. E. Kaloyeros, B. Arkles and S. J., "Low temperature plasma-assisted chemical vapor deposition of tantalum nitride from tantalum pentabromide for copper metallization," *Journal of Vacuum Science & Technology B,* vol. 17, no. 1, p. 182, 1999.

[37] K. Knapas and M. Ritala, "In situ studies on reaction mechanisms in atomic layer deposition," *Critical reviews in solid state and materials sciences,* vol. 38:3, pp. 167-

202, 2013.

[38] K.-E. Elers, V. Saanila, P. J. Soininen, W.-M. Li, J. T. Kostamo, S. Haukka, J. Juhanoja and W. F. A. Besling, "Diffusion barrier deposition on a copper surface by atomic layer deposition," *Chemical Vapor Deposition,* vol. 8, no. 4, pp. 149-153, 2002.

[39] H.-E. Cheng, W.-J. Lee and C.-M. Hsu, "The effect of deposition temperature on the properties of TiN diffusion barriers prepared by atomic layer chemical vapor deposition," *Thin Solid Films,* vol. 485, pp. 59-65, 2005.

[40] H.-E. Cheng and W.-J. Lee, "Properties of TiN films grown by atomic-layer chemical vapor deposition with a modified gasous-pulse sequence," *Materials Chemistry and Physics,* vol. 97, pp. 315-320, 2006.

[41] K. Choi, P. Lysaght, H. Alshareef, C. Huffman, H.-C. Wen, R. Harris, H. Luan, P.-Y. Hung, C. Sparks, M. Cruz, K. Matthews, P. Majhi and B. H. Lee, "Growth mechanism of TiN film on dielectric films and the effects on the work function," *Thin Solid Films,* vol. 486, pp. 141-144, 2005.

[42] C. H. Ahn, S. G. Cho, H. J. Lee, K. H. Park and S. H. Jeong, "Characteristics of TiN thin films grown by ALD using TiCl4 and NH3," *Metals and Materials International,* vol. 7, no. 6, pp. 621-625, 2001.

[43] H. Jeon, J.-W. Lee, K. Y.-D., D.-S. Kim and K.-S. Yi, "Study on the characteristics of TiN thin film deposited by the atomic layer chemical vapor deposition method," *Journal of Vacuum Science & Technology A,* vol. 18, no. 4, pp. 1595-1598, 2000.

[44] J. Kim, H. Hong, S. Ghosh, K.-Y. Oh and C. Lee, "Physical properties of highly conformal TiN thin films grown by atomic layer deposition," *Japanese Journal of Applied Physics,* vol. 42, pp. 1375-1379, 2003.

[45] J. Uhm and H. Jeon, "TiN diffusion barrier grown by atomic layer deposition method for Cu metallization," *Japanese Journal of Applied Physics,* vol. 40, pp. 4657-4660, 2001.

[46] M. Ritala, T. Asikainen, M. Leskelä, J. Jokinen, R. Lappalainen, M. Utriainen, L. Niinistö and E. Ristolainen, "Effects of intermediate zinc pulses on properties of TiN and NbN

films deposited by atomic layer epitaxy," *Applied Surface Science,* vol. 120, pp. 199-212, 1997.

[47] S. B. S. Heil, E. Langereis, F. Roozeboom, M. C. M. van de Sanden and W. M. M. Kessels, "Low-temperature deposition of TiN by plasma-assisted atomic layer deposition," *Journal of The Electrochemical Society,* vol. 153:11, pp. G956-G965, 2006.

[48] J.-S. Park, S.-W. Kang and H. Kim, "Growth mechanism and diffusion barrier property of plasma-enhanced atomic layer deposition Ti-Si-N thin films," *Journal of Vacuum Science & Technology B,* vol. 24, no. 3, p. 1327, 2006.

[49] J.-D. Kwon and J.-S. Park, "Investigating the TiN film quality and growth behaviour for plasma-enhanced atomic layer deposition using TiCl4 and N2/H2/Ar radicals," *Journal of the Korean Physical Society,* vol. 57, no. 4, pp. 806-811, 2010.

[50] S. Heil, E. Langereis, A. Kemmeren, F. Roozeboom, M. C. M. van de Sanden and W. M. M. Kessels, "Plasma-assisted atomic layer deposition of TiN monitored by in situ spectroscopic ellipsometry," *Journal of Vacuum Science & Technology A,* vol. 23, no. 4, p. L5, 2005.

[51] K.-E. Elers, J. Winkler, K. Weeks and S. Marcus, "TiCl4 as a precursor in the TiN deposition by ALD and PEALD," *Journal of The Electrochemical Society,* vol. 152:8, pp. G589-G593, 2005.

[52] K.-E. Elers, M. Ritala, M. Leskelä and E. Rauhala, "NbCl5 as a precursor in atomic layer epitaxy," *Applied Surface Science,* vol. 82/83, pp. 468-474, 1994.

[53] J. Liu, J. Bao, M. Scharnberg, W. C. Kim and P. S. Ho, "Effects of surface chemistry on ALD Ta3N5 barrier formation on low-k dielectrics," *Journal of Vacuum Science & Technology A,* vol. 23, no. 4, p. 1107, 2005.

[54] J. Liu, M. Scharnber, J. Bao, J. Im and P. S. Ho, "Initial interface formation of Ta-based barriers on SiLK low dielectric constant films," *Journal of Vacuum Science & Technology B,* vol. 23, no. 4, p. 1422, 2005.

[55] M. Ritala, P. Kalsi, D. Riihelä, K. Kukli, M. Leskelä and J. Jokinen, "Controlled growth of TaN, Ta3N5 and TaOxNy thin films by atomic layer deposition," *Chemistry of Materials,* vol. 11, no. 7, pp. 1712-1718, 1999.

[56] H. Kim, A. J. Kellock and S. M. Rossnagel, "Growth of cubic-TaN thin films by plasma-enhanced atomic layer deposition," *Journal of Applied Physics,* vol. 92, no. 12, p. 7080, 2002.

[57] N. Van Hoornick, H. De Witte, T. Witters, C. Zhao, T. Conard, H. Huotari, J. Swerts, T. Schram, J. W. Maes, S. De Gendt and M. Heyns, "Evaluation of Atomic Layer Deposited NbN and NbSiN as Metal Gate Materials," *Journal of The Electrochemical Society,* vol. 153, no. 5, pp. G437-G442, 2006.

[58] P. Alén, M. Ritala, K. Arstila, J. Keinonen and M. Leskelä, "The growth and diffusion barrier properties of atomic layer deposited NbNx thin films," *Thin Solid Films,* vol. 491, pp. 235-241, 2005.

[59] T. Proslier, J. Klug, N. Becker, J. Elam and M. Pellin, "Atomic Layer Deposition of Superconductors," *ECS Transactions,* vol. 41, no. 2, pp. 237-245, 2011.

[60] M. Juppo, M. Ritala and M. Leskelä, "Use of 1,1-Dimethylhydrazine in the Atomic Layer Deposition of Transition Metal Nitride Thin Films," *Journal of The Electrochemical Society,* vol. 147, no. 9, pp. 3377-3381, 2000.

[61] J. Klug, N. Becker, N. Groll, C. Cao, M. Weimer, M. Pellin, J. Zasadzinski and T. Proslier, "Heteroepitaxy of group IV-VI nitrides by atomic layer deposition," *Applied Physics Letters,* vol. 103, p. 211602, 2013.

[62] J. Hinz, A. Bauer and L. Frey, "Analysis of NbN thin film deposition by plasma-enhanced ALD for gate electrode application," *Semiconductor Science and Technology,* vol. 25, p. 075009, 2010.

[63] M. Ziegler, L. Fritzsch, J. Day, S. Linzen, S. Anders, J. Toussaint and H.-G. Meyer, "Superconducting niobium nitride thin films deposited by metal organic plasma-enhanced atomic layer deposition," *Superconductor Science and Technology,* vol. 26, p.

025008, 2013.

[64] R. K. Roy, Design of experiments using the Taguchi approach: 16 steps to product and process improvement, New York: Wiley, 2001.

[65] S. Audisio, H. Hamed and D. Hertz, "Deposition and study of niobium coating on iron and copper substrates from reduction of NbCl5 by hydrogen or vapors of zinc," *Journal de Physique IV,* vol. 5, pp. C5-1087, 1995.

[66] S. M. Rossnagel, A. Sherman and F. Turner, "Plasma-enhanced atomic layer deposition of Ta and Ti for interconnect diffusion barriers," *Journal of Vacuum Science & Technology B,* vol. 18, no. 4, p. 2016, 2000.

[67] H. Kim and S. M. Rossnagel, "Growth kinetics and initial stage growth during plasma-enhanced Ti atomic layer deposition," *Journal of Vacuum Science & Technology A,* vol. 20, no. 3, p. 802, 2002.

[68] H. Kim, "Atomic layer deposition of metal and nitride thin films: Current research efforts and applications for semiconductor device processing," *Journal of Vacuum Science & Technology B,* vol. 21, pp. 2231-2261, 2003.

[69] H. C. M. Knoops, L. Baggetto, E. Langereis, M. C. M. van de Sanden, J. H. Klootwijk, F. Roozeboom, R. A. H. Niessen, P. H. L. Notten and W. M. M. Kessels, "Deposition of TiN and TaN by remote plasma ALD for Cu and Li diffusion barrier applications," *Journal of The Electrochemical Society,* vol. 155, no. 12, pp. G287-G294, 2008.

[70] J.-S. Park and S.-W. Kang, "Plasma-enhanced ALD of titanium-silicon-nitride using TiCl4, SiH4, and N2/H2/Ar plasma," *Electrochemical and Solid-State Letters,* vol. 7, no. 8, pp. C87-C89, 2004.

[71] F. Greer, D. Fraser, J. W. Coburn and D. B. Graves, "Fundamental beam studies of radical enhanced atomic layer deposition of TiN," *Journal of Vacuum Science & Technology A,* vol. 21, no. 1, p. 96, 2003.

[72] D. Gu, K. Tapily, H. Baumgart, G. Namkoong and R. Crooks, "Synthesis of NbN Thin Films for Superconducting Radiofrequency (SRF) Applications by Atomic Layer

Deposition to Fabricate Superconductor-Insulator-Superconductor (S-I-S) Multilayer Structures," *ECS Transactions,* vol. 33, no. 2, pp. 203-209, 2010.

[73] J. Hinz, A. Bauer, T. Thiede, R. Fischer and L. Frey, "Evaluation of NbN thin films grown by MOCVD and plasma-enhanced ALD for gate electrode application in high-k / SiO2 gate stacks," *Semiconductor Science and Technology,* vol. 25, p. 045009, 2010.

[74] P. Alén, Atomic Layer Deposition of TaN, NbN, and MoN Films for Cu Metallizations, Helsinki, 2005.

[75] J. A. Klug, T. Proslier, J. W. Elam, R. E. Cook, J. M. Hiller, H. Claus, N. G. Becker and M. J. Pellin, "Atomic Layer Deposition of Amorphous Niobium Carbide-Based Thin Film Superconductors," *The Journal of Physical Chemistry C,* no. 115, pp. 25063-25071, 2011.

[76] E. W. Deguns, M. J. Sowa, M. J. Dalberth, R. Bhatia, R. Kanjolia, D. Moser, G. M. Sundaram and J. S. Becker, "Plasma-Enabled ALD of Niobium Nitride Using an Organometallic Nb Precursor," *ECS Transactions,* vol. 33, no. 2, pp. 177-182, 2010.

[77] A.-M. Valente-Feliciano, H. Phillips, C. Reece and J. Spradlin, "SRF Multilayer structures based on NbTiN," *Proceedings of SRF2011.*

Appendix A: Compilation of deposited samples

Table 15: Compliation of deposition parameters for thermal process with $NbCl_5$ and NH_3 in the order they were deposited.

Thermal depositions using $NbCl_5$ and NH_3												
				$NbCl_5$				**NH_3**			**Other lines**	
Sample #	Reactor temperature (°C)	Substrate	Cycles	Pulse (s)	Purge (s)	Source bottle (°C)	Line flow (sccm)	Pulse (s)	Purge (s)	Line flow (sccm)	Line 1,2,3,4 flow (sccm)	Comment
1	500	4” SiO_2	1000	0.5	10	120	200	0.1	12	80	40	Film only in middle of the wafer
2	500	4“ SiO_2	1000	2 x 0.5	10	120	250	0.1	12	80	40	No film
3	500	4” SiO_2	1000	2 x 1.5	10	120	200	0.1	12	80	40	Asymmetric film and mostly at edges
4	500	4” SiO_2	1000	1.5	10	120	250	0.1	12	80	40	Film only in middle of the wafer
5	400	4” SiO_2	3330	1.5	5	125	250	1	6	80	40	Visibly uniform film
6	400	4” SiO_2	3330	1.5	3	125	250	1	3	80	40	Visibly uniform film
7	400	4” SiO_2	1500	1.5	5	125	250	1	6	80	40	Visibly uniform film
8	400	4” SiO_2	1500	1.5	5	128	250	0.5	6	80	40	Slightly thinner film in south

				$NbCl_5$				NH_3			Other lines	
Sample #	Reactor temperature (°C)	Substrate	Cycles	Pulse (s)	Purge (s)	Source bottle (°C)	Line 4 flow (sccm)	Pulse (s)	Purge (s)	Line 6 flow (sccm)	Line 1,2,3,5 flow (sccm)	Comment
9	475	4” SiO_2	1500	1.5	5	125	250	0.5	6	80	40	Slightly thinner film in south
10	475	4” SiO_2	1500	1.5	5	128	250	1	6	80	40	Visibly uniform film
11	475	4” SiO_2	1500	1.5	5	125	250	1	6	80	40	Visibly uniform film
12	500	6” SiO_2	1500	1.5	5	125	200	1	6	80	40	Film didn’t grow from SW to E
13	500	6” SiO_2	1500	1.5	5	125	275	1	6	80	40	Film area shrank, does not reach edge
14	500	6” SiO_2	500	1.5	5	125	150	1	6	80	40	Center point of film growth shifted towards N and no growth from SW to E
15	500	6” SiO_2	500	1.5	5	125	200	1	6	100	40	Slightly smaller film growth area than in S14
16	500	6” SiO_2	500	1.5	5	125	200	1	6	80	1&2 20 3&5 60	Run failed

Sample #	Reactor temperature (°C)	Substrate	Cycles	$NbCl_5$ Pulse (s)	Purge (s)	Source bottle (°C)	Line 4 flow (sccm)	NH_3 Pulse (s)	Purge (s)	Line 6 flow (sccm)	Other lines Line 1,2,3,5 flow (sccm)	Comment
17	500	6" SiO_2	500	1.5	5	125	200	1	6	80	1&2 20 3&5 60	Asymmetric growth and film does not reach edges
18	500	6" SiO_2	1500	1.5	5	125	250	1	6	80	40	Growth does not reach edges and off centered growth
19	475	6" SiO_2	1500	1.5	5	125	250	1	6	80	40	Growth does not reach edges
20	475	4" SiO_2	1500	1.5	5	125	200	1	6	80	40	Visibly thinner in S
21	475	4" SiO_2	500	1.5	5	125	200	1	6	80	40	Visibly thinner in S
MS1	400	4" Si	3600	1.5	5	125	200	1	6	80	40	Visibly uniform film
MS2	450	4" Si	3600	1.5	5	125	200	1	6	80	40	Visibly thinner in S
MS3	500	4" Si	3600	1.5	5	125	200	1	6	80	40	Film did not reach wafer edge in S
MS4	500	4" Si	1800	1.5	5	125	200	1	6	80	40	Film did not reach wafer edge in S
MS5	500	4" Si	900	1.5	5	125	200	1	6	80	40	Did not reach wafer edge in S

Sample #	Reactor temperature (°C)	Substrate	Cycles	$NbCl_5$ Pulse (s)	Purge (s)	Source bottle (°C)	Line 4 flow (sccm)	NH_3 Pulse (s)	Purge (s)	Line 6 flow (sccm)	Other lines Line 1,2,3,5 flow (sccm)	Comment
22	500	4” SiO_2	900	1.5	5	125	200	1	6	80	40	Run failed
23	500	4” SiO_2	900	1.5	5	125	200	1	6	80	40	Visibly uniform film
24	500	4” SiO_2	900	1.5	5	135	200	1	6	80	40	Run failed
25	500	4” SiO_2	900	1.5	5	135	200	1	6	80	40	Visibly uniform film
27	500	4” SiO_2	900	1.5	5	135	200	1	10	80	40	Visibly uniform film
28	500	4” SiO_2	900	1.5	5	135	200	1	15	80	40	Visibly uniform film
29	500	4” SiO_2	900	1.5	10	135	200	1	15	80	40	Visibly uniform film
31	500	4” SiO_2	900	0.5	5	135	200	1	10	80	40	Visibly uniform film
32	500	4” SiO_2	900	2.5	5	135	200	1	10	80	40	Visibly uniform film
33	500	4” SiO_2	900	1.5	5	140	200	1	10	80	40	Visibly uniform film
34	500	4” SiO_2	900	2.5	5	135	200	1.5	10	80	40	Visibly uniform film
35	500	4” SiO_2	900	2.5	5	135	200	0.5	10	80	40	Visibly uniform film
36	500	4” SiO_2	900	2.5	5	135	200	1.5	10	80	40	Visibly uniform film

Table 16: Deposition parameters used for ABC process development.

Thermal ABC process																
					$NbCl_5$				NH_3			H_2			Other lines	
Sample #	ALD Cycle	Reactor temperature (°C)	Substrate	Cycles	Pulse (s)	Purge (s)	Source bottle (°C)	Line 4 flow (sccm)	Pulse (s)	Purge (s)	Line 6 flow (sccm)	Pulse (s)	Purge (s)	Line 7 flow	Line 1,2,3,5 flow (sccm)	Comment
40	$NbCl_5$ ->H_2 ->NH_3	500	4” SiO_2	900	1.5	5	135	200	1	6	80	3	5	Ar 40 H_2 53	40	Deposition mostly on edges and more than usual on backside
45	$NbCl_5$ ->NH_2 ->H_3	500	4” SiO_2	900	1.5	5	135	200	1	6	80	3	5	Ar 40 H_2 53	40	Visibly uniform film, but on the other hand similar to the one with only ammonia
46	$NbCl_5$ ->NH_3	500	4” SiO_2	900	1.5	5	135	200	1	6	80	0	0	Ar 40 H_2 0	40	Visibly uniform film

Table 17: Deposition parameters for all plasma processes.

Plasma processes													
N_2/H_2-plasma				$NbCl_5$				N_2/H_2				Other lines	
Sample #	Reactor temperature (°C)	Substrate	Cycles	Pulse (s)	Purge (s)	Source bottle (°C)	Line 4 flow (sccm)	Pulse (pre-stab. /RF on/ post-stab.) (s)	RF power (W)	Purge (s)	Line 7 flow ($Ar/N_2/H_2$) (sccm)	Line 1,2,3,5,6 flow (sccm)	Comment
26	500	4” SiO_2	900	1.5	5	135	200	1/25/1	1000	4	80/35/30	40	Visibly uniform
37	500	4” SiO_2	400	1.5	5	135	200	1/25/1	1000	4	80/35/30	40	Visibly uniform
39	500	4” SiO_2	400	1.5	5	135	200	1/25/1	1000	4	80/5.3/53	40	Visibly uniform
41	500	4” SiO_2	400	1.5	5	135	200	1/25/1	1500	4	80/5.3/53	40	
43	500	4” SiO_2	400	1.5	5	135	200	1/15/0.5	1000	4	80/5.3/53	40	
44	500	4” SiO_2	400	1.5	5	135	200	1/15/0.5	500	4	80/5.3/53	40	High sheet resistance
47	500	4” AlN	400	1.5	5	135	200	1/15/9	1000	4	80/5.3/53	40	Mistake with parameters
48	500	4” AlN	400	1.5	5	135	200	1/25/1	1000	4	80/5.3/53	40	Rerun on S47 Visibly uniform

H_2-plasma				$NbCl_5$				H_2				Other lines	
Sample #	Reactor temperature (°C)	Substrate	Cycles	Pulse (s)	Purge (s)	Source bottle (°C)	Line 4 flow (sccm)	Pulse (pre-stab. /RF on/ post-stab.) (s)	RF power (W)	Purge (s)	Line 7 flow (Ar /H_2) (sccm)	Line 1,2,3,5,6 flow (sccm)	Comment
30	500	4" SiO_2	900	1.5	5	135	200	1/25/1	1000	4	80/30	40	Visibly uniform
38	500	4" SiO_2	400	1.5	5	135	200	1/25/1	2000	4	80/30	40	Highly resistive yellow film produced
49	500	4" SiO_2	1200	1.5	5	135	200	1/25/1	1000	4	80/53	40	Visibly uniform
NH_3-plasma				**$NbCl_5$**				**NH_3**				**Other lines**	
Sample #	Reactor temperature (°C)	Substrate	Cycles	Pulse (s)	Purge (s)	Source bottle (°C)	Line 4 flow (sccm)	Pulse (pre-stab. /RF on/ post-stab.) (s)	RF power (W)	Purge (s)	Line 7 flow (Ar /NH_3) (sccm)	Line 1,2,3,5,6 flow (sccm)	Comment
42	500	4" SiO_2	900	1.5	5	135	200	1/15/0.5	1000	4	40/32	40	Visibly uniform

Appendix B: Thickness and resistivity of samples 7-11

Table 18: Thickness and resistivity for samples 7-11. Thickness is determined by XRR for samples 7-10. Thickness of sample 11 is approximated based on these.

	Sample 7		Sample 8		Sample 9		Sample 10		Sample 11	
	t (nm)	ρ (μΩcm)	t (nm)	ρ (μΩcm)	t (nm)	ρ (μΩcm)	t (nm)	ρ (μΩcm)	t (nm)	ρ (μΩcm)
N	39.0	1770	32.0	2370	40.0	910	40.0	920	40	800
C	42.6	1700	36.5	2050	44.5	830	42.5	920	40	780
S	38.5	1620	35.0	1900	40.5	980	39.5	910	40	850
W	38	1460	38.0	1780	43.2	850	42.5	890	40	760
E	39.2	1760	33.5	2270	40.5	940	40.3	950	40	870
Ave.	39.5	1660	35.0	2070	41.7	900	41.0	920	40	810
σ	1.8	130	2.4	250	2.0	60	1.4	20	0	50

Appendix C: ToF-ERDA depth profiles for samples MS1-5

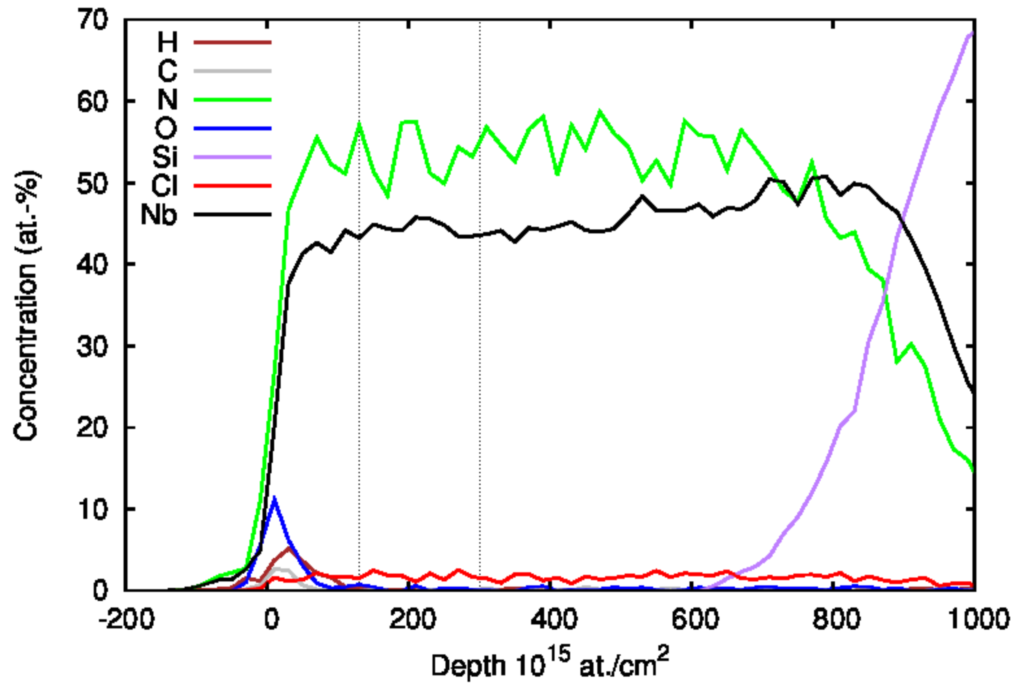

Figure 16: ToF-ERDA depth profile for sample MS1.

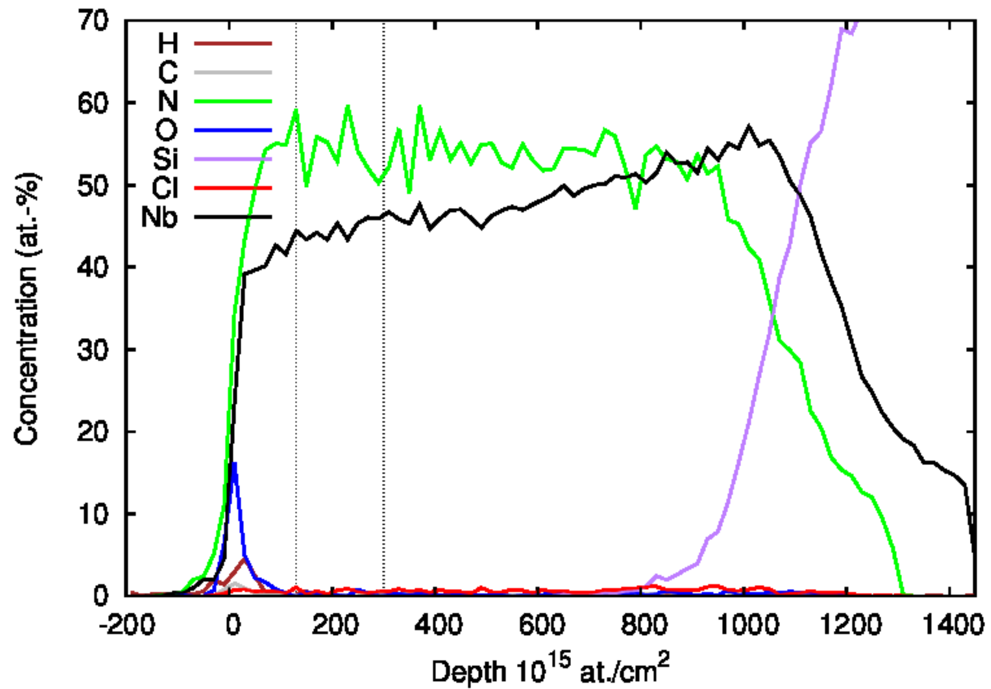

Figure 17: ToF-ERDA depth profile for sample MS2.

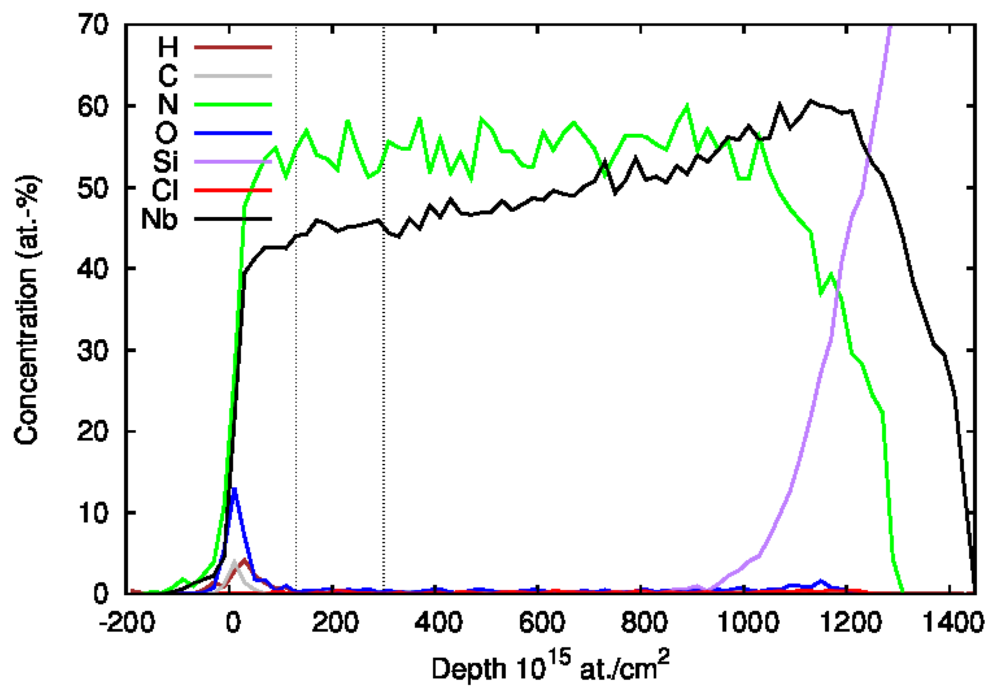

Figure 18: ToF-ERDA depth profile for sample MS3.

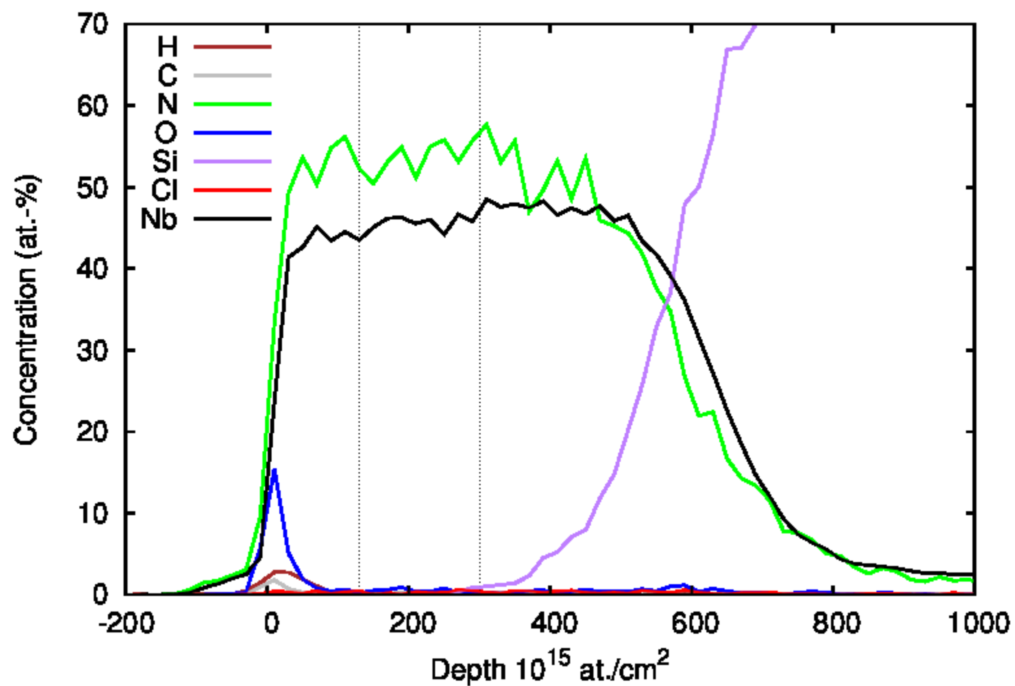

Figure 19: ToF-ERDA depth profile for sample M4.

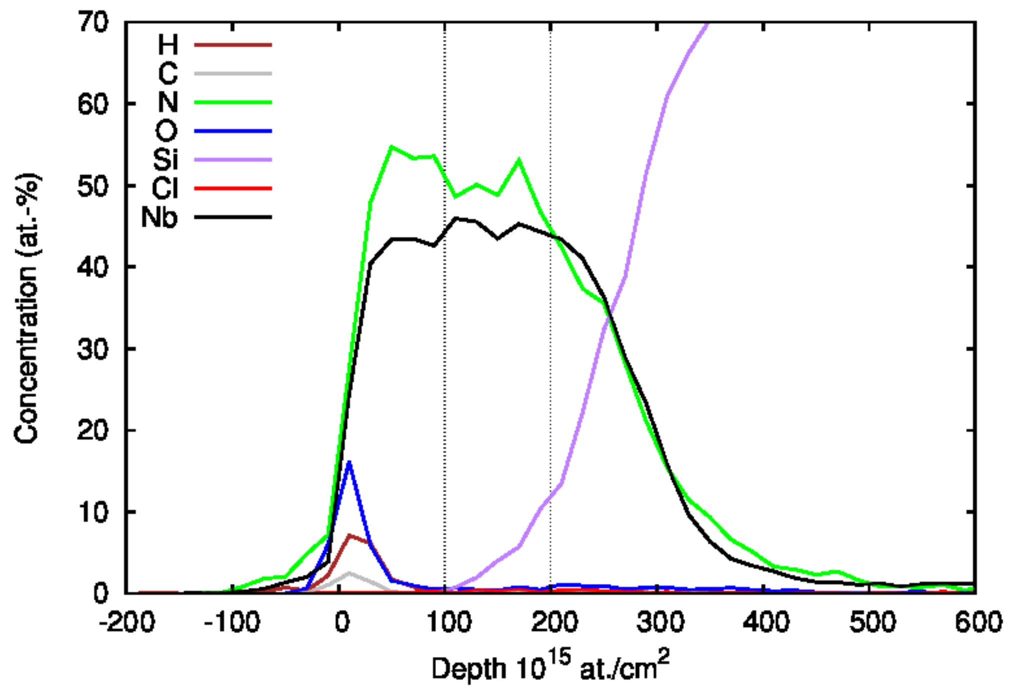

Figure 20: ToF-ERDA depth profile for sample